1 Rheology of disperse systems

N. Willenbacher and K. Georgieva

1.1 Introduction

Rheology of disperse systems is an extremely important processing parameter. Being able to characterize and manipulate the flow behavior of dispersions one can ensure their optimal performance. Automotive coatings, for example, should exhibit a distinct low-shear viscosity necessary to provide good leveling but to avoid sagging at the same time. Then a strong degree of shear thinning is needed in order to guarantee good pump- and sprayability. The rheological properties of dispersions, especially at high solid content, are complex and strongly dependent on the applied forces. Adding particles does not simply increase the viscosity of the liquid as a result of the hydrodynamic disturbance of the flow; it also can be a reason for deviation from the Newtonian behavior including shear rate dependent viscosity, elasticity and time dependent rheological behavior. Colloidal dispersions at moderate volume fraction normally flow like shear-thinning, low viscous liquids. At high concentrations dispersions often behave as solids and require a finite stress to deform the structural network and then start to flow. The microstructure deformed under stress usually can not recover immediately from large strains since the colloidal interactions governing the microstructure have a short range and decrease with increasing the interparticle separation. Depending whether the colloidal interactions are attractive or repulsive the particles can form different structures which determine the rheological behavior of the material. In the case of attractive particle interactions loose flocs with fractal structure can be formed immobilizing part of the continuous phase thus leading to larger effective particle volume fraction and correspondingly to increase of viscosity. Above a critical volume fraction a sample-spanning network forms, which results in a highly elastic, gel-like behavior and an apparent yield stress. Shear-induced breakup and recovery of floc structure leads to thixotropic behavior. Electrostatic or steric repulsion between particles define an excluded volume which is not accessible by another particle leading to crystalline or gel-like state at particle concentrations lower than the maximum packing fraction.

Characterization of the microstructure and flow properties of dispersions is essential for the understanding and controlling their rheological behavior. In this chapter we first introduce methods and techniques for standard rheological tests and then characterize the rheology of hard

spheres, repulsive and attractive particles. The effect of particle size distribution on the rheology of highly concentrated dispersions and the shear thickening phenomenon will be discussed with respect to the influence of colloidal interactions on these phenomena. Finally, typical features of emulsion rheology and the flow behavior of more complex fluids based on emulsions or suspensions will be dicussed.

1.2 Basics of Rheology

According to its definition, Rheology is the science of the deformation and flow of mater. The rheological behavior of materials can be regarded as being between two extremes: Newtonian viscous fluids, typically low-molecular liquids, and Hookean elastic solids, like for example rubber. However, most of the real materials exhibit mechanical behavior with both viscous and elastic characteristics. Such materials are termed viscoelastic. Before considering the more complex viscoelastic behavior, let us first elucidate the flow properties of ideally viscous and ideally elastic materials.

Isaac Newton first introduced the notion of viscosity as a constant of proportionality between the force per unit area (shear stress) required to produce a steady simple shear flow and the resulting velocity gradient in the direction perpendicular to the flow direction (shear rate):

[eq_001]

Equation 1.1

$$\sigma = \eta\dot{\gamma}$$

where σ is the shear stress, η the viscosity and the $\dot{\gamma}$ is the shear rate. A fluid that obeys this linear relation is called Newtonian, which means that viscosity is independent of shear rate for the shear rates applied. Glycerine, water and some mineral oils are typical examples for Newtonian liquids. The Newtonian behavior is also characterized by constant viscosity with respect to the time of shearing and an immediate relaxation of the shear stress after the shearing is stopped. Furthermore the viscosities measured in different types of deformation are always proportional to one another

Materials such as dispersions, emulsions and polymer solutions often depart from the Newtonian behavior and the viscosity is found to decrease or increase with increasing shear rate, referring to shear thinning and shear thickening respectively. The general shape of the curves

representing the variation of viscosity as a function of shear rate and the corresponding graphs of shear stress as a function of shear rate are shown in Figure 1.1a–b

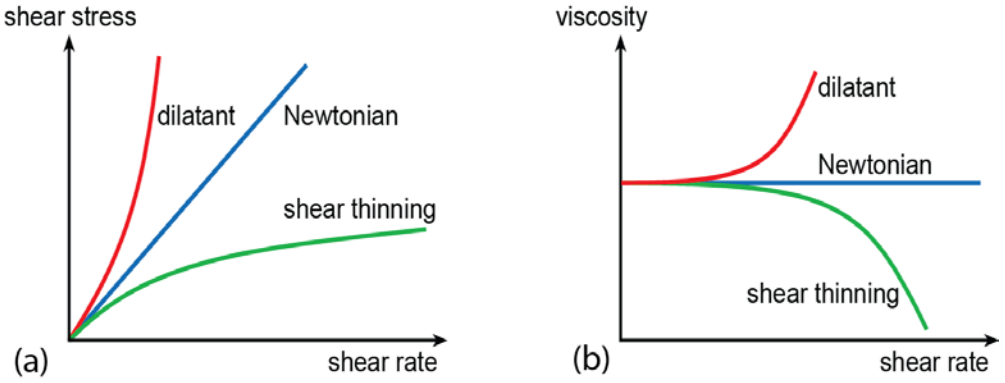

[Fig_001]

Figure 1.1a–b Typical flow curves for Newtonian, shear-thinning and shear thickening fluids **a** viscosity as a function of shear arte **b** shear stress as a function of shear rate

Materials with a yield stress behave as solids at rest and start to flow only when the applied external force overcome the internal structural forces. Concentrated dispersions with attractive interactions, emulsions and foams, clay suspensions, automotive coatings and ketchup are typical examples for materials with yield point. A characteristic flow curve showing the yield stress is schematically displayed in Fig. Note that there are various methods for yield point determination and the measured value may differ depending on the method and instrument used.

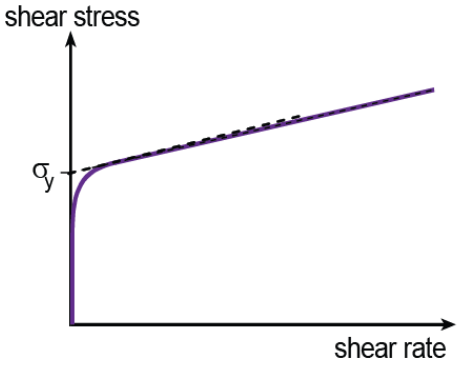

[Fig_002]

Figure 1.2 Flow curve of a material with a yield stress σ_y

The flow history of a material also should be taken into account when making predictions of the flow behavior. Two important phenomena related to the time-dependent flow behavior are the thixotropy and rheopexy. For sample showing thixotropic behavior the viscosity gradually decreases with time under constant shear rate followed by a gradual structural regeneration when the stress is removed. The thixotropic behavior can be identified measuring the shear stress as a

function of increasing and decreasing shear rate. Fig shows a hysteresis typical for thixotropic dispersions. Materials exhibiting a rheopectic behavior show an increase of the viscosity with time at constant shear rate. Fluids showing rheopectic behavior are much less common than thixotropic materials.

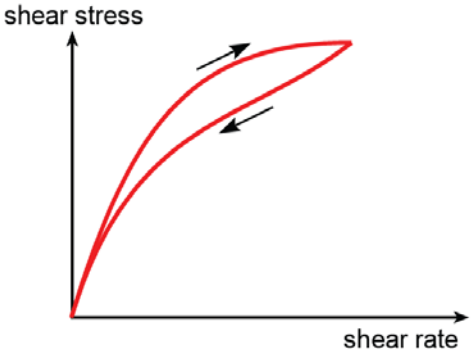

[Fig_003]

Figure 1.3 Flow curve of a thixotropic material

So far we have considered the flow behavior of viscous fluids in terms of the Newton's law and non-linear change of viscosity with applied stress which can occur either instantaneously or over a long period of time. At the other extreme is the ideal elastic behavior of solids which can be described by the Hooke's law of elasticity:

[eq_002]

Equation 1.2

$$\sigma = G\gamma$$

where γ is the deformation (also termed strain) and G is the shear modulus which reveals information about the rigidity of a material. The shear modulus of an idealelastic solid is independent of the shear stress and duration of the shear load. As soon as the deformation is reached, no further motion occurs. In contrast, viscoelastic materials deform at constant stress partially simultaneously, partially continuously over time. Thus, the time dependent stress relaxation is used to measure the visoelasticity of materials. When the stress relaxation is proportional to the strain we are talking about the so called linear viscoelastic regime. Above a critical strain the microstructure of the sample breakup and the shear modulus becomes strain dependent. This is so called nonlinear viscoelastic regime.

Dynamic test or small amplitude oscillatory shear (SAOS) test is the most widely used rheological measurement to investigate the linear viscoelastic behavior of a fluid, since it is sensitive to the microstructure, easy to use and has a sound mathematical background. When oscillatory shear strain is applied to a viscoelastic material it will be deformed sinusoidally by a deformation $\gamma(t)$ with amplitude γ_0 and angular frequency ω:

[eq_003]

Equation 1.3

$$\gamma(t) = \gamma_0 \sin(\omega t)$$

where t denotes the time. Hence the shear rate can be expressed as the time derivative of the shear strain as follows:

[eq_004]

Equation 1.4

$$\dot{\gamma}(t) = \frac{d\gamma(t)}{dt} = \gamma_0 \omega \cos(\omega t)$$

The oscillating system responds with sinusoidal course of shear stress $\sigma(t)$ with amplitude σ_0 and angular frequency ω, but phase shifted by an angle δ compared to the presented sine curve:

[eq_005]

Equation 1.5

$$\sigma(t) = \sigma_0 \sin(\omega t + \delta)$$

Depending on material behavior, the phase shift angle δ occurs between 0° and 90°. For ideal elastic materials the phase shift disappear, i.e. $\delta = 0°$ while for ideal viscous liquids $\delta = 90°$. In oscillatory shear experiment the shear modulus is written in complex form:

[eq_006]

Equation 1.6

$$G^*(\omega) = \frac{\sigma(t)}{\gamma(t)}$$

The complex shear modulus G* consists of two components: the storage modulus G' and loss modulus G":

[eq_007]

Equation 1.7

$$G^*(\omega) = G'(\omega) + iG''(\omega)$$

The G'-value is a measure of the energy stored by the material during the cycle of deformation and represents the elastic behavior of the material, while G" is measure of the energy dissipated or lost as heat during the shear process and represents the viscous behavior of a test material. The G'- and G" can be expressed as sine and cosine function of the phase shift angle δ as follows:

[eq_008]

Equation 1.8

$$G'(\omega) = \frac{\sigma_0}{\gamma_0}\cos\delta$$

[eq_009]

Equation 1.9

$$G''(\omega) = \frac{\sigma_0}{\gamma_0}\sin\delta$$

Hence the tangent of the phase shift δ can be defined as the ratio of loss and storage modulus:

[eq_010]

Equation 1.10

$$\tan\delta = \frac{G''(\omega)}{G'(\omega)}$$

Analogous to the complex shear modulus we can express a complex viscosity η*, defined as follows:

[eq_011]

Equation 1.11

$$\eta^*(\omega) = \frac{\sigma(t)}{\dot{\gamma}(t)} = \eta'(\omega) + i\eta''(\omega)$$

where η' represents the viscous behavior and η" the elastic part of the complex viscosity. The complex viscosity may be more convenient dealing with liquids but we can readily convert to the dynamic moduli:

[eq_012]

Equation 1.12

$$\eta'(\omega) = \frac{G''(\omega)}{\omega}$$

[eq_013]

Equation 1.13

$$\eta''(\omega) = \frac{G'(\omega)}{\omega}$$

The viscoelastic properties of a fluid can be characterized by oscillatory measurements, performing amplitude- and frequency sweep. The oscillatory test of an unknown sample should be started with an amplitude sweep, i.e. variation of the amplitude at constant frequency. Up to a limiting strain γ_y the structure of the tested fluid remains stable and G′ as well as G′′ is independent of the strain amplitude. Above the limiting amplitude of deformation the structure of the sample has been changed and G' as well as G" decrease with increasing deformation. The

linear viscoelastic range may depend on the angular frequency ω. At higher frequencies many materials show higher rigidity and more brittle behavior, therefore lower limiting amplitude γ_y.

Frequency sweeps are used to examine the time dependent shear behavior. For this purpose the frequency is varied using constant amplitude within the linear viscoelastic range. At appropriately high angular frequency ω, i.e. short term behavior, the samples show an increased rigidity and hence G' > G". At lower frequencies (long term behavior) the microstructure is more flexible and the viscous behavior dominates, correspondingly G" > G'.

1.3 Experimental Methods of Rheology

Experimental methods to determine the flow properties of fluids are termed rheometers, while measuring systems used for viscosity measurements are specified as viscometer. The rheometers can be categorized by the flow type in which materials properties are investigated: simple shear and extensional flow. The shear rheometers can be divided into rotational, in which the shear is generated between fixed and moving solid surface, and pressure driven like the capillary rheometer, in which the shear is generated by a pressure difference over the channel through which the material flows. Extensional rheometers are relatively less developed than shear rheometers because of the difficulties to generate homogeneous extensional flow especially for liquids with low viscosity. Many different experimental techniques have been developed to characterize the eleongational properties of fluids and predict their processing and application behaviour. The most successful commercially available instrument is the capillary breakup extensional rheometer (CaBER). The thinning and breakup of fluid filament controlled by the balance between surface tension and viscoelastic force provides valuable information about materials rheological properties in an elongational flow. However, further development and better understanding of the CaBER experiments is necessary

1.3.1 Rotational Rheometry

In rotational instruments the rheological properties of materials can be characterized in a steady simple shear flow with homogeneous regime of deformation. Basically there are two different regimes of deformation: imposition of constant rotational speed or constant torque, corresponding to controlled shear rate and controlled shear stress, respectively. Moreover, many rotational rheometers are capable to impose harmonic oscillations for measuring the viscoelastic material properties. Three types of measuring systems are commonly used in the modern

rotational rheometry, namely concentric cylinder, cone-and-plate and parallel-plate. Typically shear rates that can be measured with rotational rheometers are in the range 10^{-3} to10^{3} s^{-1}

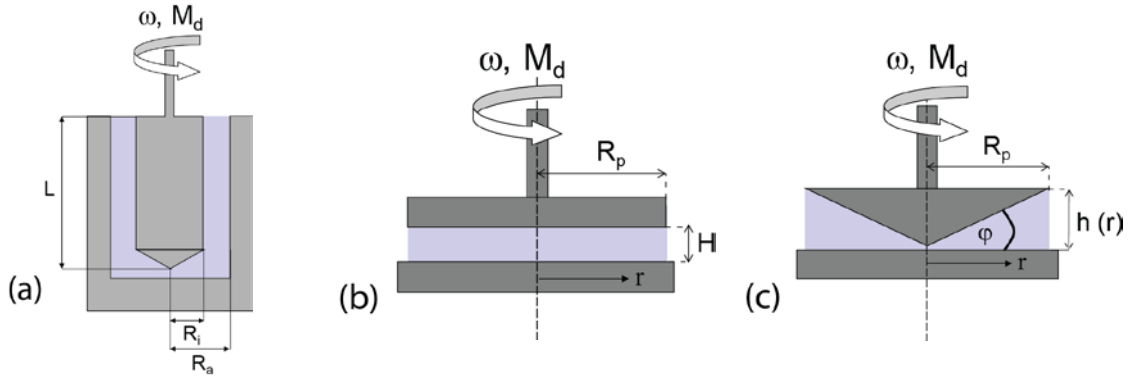

[Fig_004]

Figure 1.4a–c Schematic representation of **a** concentric cylinder **b** parallel-plate and **c** cone-and-plate measuring system

1.3.1.1 Concentric Cylinder Measuring System

As shown in Figure 1.4a, a cylinder measuring system consists of outer cylinder (cup) and inner cylinder (bob). There are two modes of operation depending on that if the cup or the bob is rotating. The Searle method corresponds to a rotating bob and stationary cup, while in the Couette mode the cup is set in motion and the bob is fixed. The gap between the two concentric cylinders should be small enough so that the sample confined in the gap experiences a constant shear rate. This requirement is fulfilled and the gap is classified as “narrow” when the ratio of the outer to the inner cylinder radius is greater than 0.97. On the other side, the narrow gap concentric cylinder measuring systems are associated with difficulties when investigating suspensions of relatively large particles. In this case, wider gap viscometers are preferable, but the inaccuracy involved due shear rate changes across the gap should be taken into account.

Consider the flow of a sample enclosed in the gap between the cup with radius R_a and the bob with radius R_i. When the bob is rotating at angular velocity ω the shear rate is given by:

[eq_014]

Equation 1.14

$$\dot{\gamma} = 2\omega \frac{R_a^2}{R_a^2 - R_i^2}$$

If the torque measured on the bob is M_d, the shear stress σ in the sample is given by:

[eq_015]

Equation 1.15

$$\sigma = \frac{M_d}{2\pi R_i^2 L}$$

where L is the effective immersed length of the bob. Having the shear rate $\dot{\gamma}$ and shear stress σ, sample viscosity η can be calculated according to the Newton's postulate (Equation 1.1). For these calculations we ignore any end effects, which are actually likely to occur as a result of the different shearing conditions in the liquid covering the ends of the cylinders. In order to minimize the end effect the ratio of the length L to the gap between cylinders is maintained greater than 100 and the shape of the bottom of the bob is designed as a cone with an angle α, which is chosen so that the shear rate in the bottom match the that in the narrow gap between the concentric cylinders.

The concentric cylinder measuring system is especially suitable for low-viscous liquids, since they cannot flow off the shear gap. Other advantages of this geometry are that annular gap remains fill even in the case of samples showing the Weissenber effect and the sample evaporation can be easily prevented by a cover or a solvent trap. Furthermore, the temperature of the sample can be easily controlled due to the large contact area.

1.3.1.2 Parallel-Plate Measuring system

The parallel plate geometry is shown in Figure 1.4b. The sample confined in the gap H between the two coaxial parallel plates is sheared by the rotation of one of the plates at angular velocity ω. Thereby the circumferential velocity *v* depends on the distance between the plates h and distance r from the rotational axis:

[eq_016]

Equation 1.16

$$v(r,h) = \omega r \frac{h}{H}$$

and thus:

[eq_017]

Equation 1.17

$$\dot{\gamma}(r) = \frac{r\omega}{H}$$

The shear rate $\dot{\gamma}$ at a constant ω is not constant within the entire shear gap. It increases from zero at the center (r = 0) to maximum at the rim of the plate (r = R_p). Typically the calculations and analysis of rheological results in parallel-plate measuring systems are related to the maximum shear rate value at the rim of the plate. The shear rate can be varied in a wide range by changing the gap height H and the angular velocity ω.

The shear stress σ is a function of the shear rate $\dot{\gamma}$, which is not constant within the gap. Thus to relate the shear stress to the total torque an expression for the $\sigma(\dot{\gamma})$ dependence is necessary. In the case of Newtonian liquid the shear stress depends linearly on the shear rate and can be expressed as follows:

[eq_018]

Equation 1.18

$$\sigma(R) = \frac{2M_d}{\pi R_p^{\,3}}$$

This expression is called apparent shear stress. Geisekus and Langer [1](1977) developed a simple approximate single point method to correct the shear rate data, based on the idea that the true and apparent shear stress must equal at some position near the wall. It was found that this occurs at the position where $r/R_p = 0.76$ and holds for a wide range of liquids.

The parallel-plate measuring system makes possible measurements of suspensions with relative large particles by using large gap heights. On the other hand, operating at small gaps viscosity can obtained at relatively high shear rates. Small gaps also allow for reduction of errors due to edge effects and secondary flows.

1.3.1.3 Cone-and-Plate Measuring System

A cone-and-plate geometry is shown schematically in Figure 1.4c. The sample is contained between a rotating relative flat cone and a stationary plate. Note that the apex of the cone is cut

off to avoid friction between the rotating cone and the lower plate. The gap angle φ is usually between 0.3° and 6° and the cone and plate radius R_p is between 10 to 30 mm. The gap h is increasing with the distance r from the rotation axis and reaches it maximum value at the edge of the cone:

[eq_019]

Equation 1.19

$$h(r) = r \tan \varphi$$

The circumferential velocity *v* is also increasing with increasing the distance r:

[eq_020]

Equation 1.20

$$v(r) = r\omega$$

Hence the shear rate is constant within the entire gap and does not depend on the radius r:

[eq_021]

Equation 1.21

$$\dot{\gamma} = \frac{dv(r)}{dh(r)} = \frac{\omega}{\tan \varphi} \approx \frac{\omega}{\varphi}$$

The shear stress measured by the torque M_d on the cone is given by:

[eq_022]

Equation 1.22

$$\sigma = \frac{3M_d}{2\pi R_p^3}$$

A great advantage of the cone-and-plate geometry is that the shear rate remains constant und thus provides homogenous shear conditions in the entire shear gap. Limited maximum particle

size of the investigated sample, difficulties with avoiding solvent evaporation and temperature gradients in the sample are typical disadvantages of the cone-and-plate measuring system

1.3.2 Capillary Rheometer

A schematic diagram of a piston driven capillary rheometer is show in Fig. A piston drives the sample to flow at constant flow rate from a reservoir through a straight capillary tube of radius R and length L. The measured pressure drop (Δp) and flow rate (Q) over the capillary are used to evaluate the shear stress, shear rate and correspondingly viscosity of the sample.

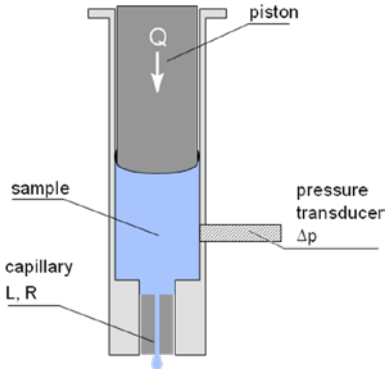

[Fig_005]

Figure 1.5 Schematic representation of a controlled flow rate capillary rheometer

Pressure driven flows through a capillary have maximum velocity at the center and maximum shear rate at the wall of the capillary, consequently the deformation is essentially inhomogeneous. Assuming Newtonian liquid and fully developed, incompressible, laminar, steady flow, the apparent wall shear stress σ_a is related to the pressure drop Δp by:

[eq_023]

Equation 1.23

$$\sigma_a = \frac{\Delta p R}{2L}$$

and the apparent or Newtonian shear rate at the wall can be calculated on the basis of measured flow rate according to:

[eq_024]

Equation 1.24

$$\dot{\gamma}_a = \frac{4Q}{\pi R^3}$$

Therefore we can evaluate the viscosity in terms of an apparent viscosity based on the Newton's postulate (Equation 1.1).

To get the true shear rate in the case of non-Newtonian fluids the Weissenberg-Rabinowitch correction [2] for non parabolic velocity profile should be taken into account. A more simple method to determine the true shear rate has been developed by Giesekus and Langer[1] as well as Schümmer[3]. Their single point method is based on the idea that the true and apparent shear rate must be equivalent at a certain radial position near the wall and thus the true shear rate $\dot{\gamma}$ is given simply by:

[eq_025]

Equation 1.25

$$\dot{\gamma} = 0.83\dot{\gamma}_a$$

Note that this approximation does no differ significantly from the Weissenberg-Rabinowitsch correction.

Other possible sources of error in the capillary experiment are entrance effects, slippage at the capillary wall and viscous heating effects. The entrance effect is associated with not fully developed flow at the capillary entrance which can be minimized using long capillary dies with ratio $L/R \geq 60$[2]. Furthermore, the pressure drop Δp is difficult to measure directly in the capillary therefore it is usually detected by a transducer mounted above the entrance of the capillary. Hence the measured pressure includes not only the pressure loss due to the laminar flow in the die but also the entrance pressure loss due to the convergence of the flow at the capillary entrance. Buggley[4] proposed a correction that accounts for the additional pressure loss at the entrance but in many practical applications it is sufficient to use capillary dies with L/R ratio large enough.

For highly concentrated suspensions wall slip effects, due to shear induced particle migration and specific particle-wall interactions has to be considered. It is possible to correct the apparent wall shear rate according to the procedure developed by Mooney [5] comparing flow curves determined with dies of different radii but similar L/R.

The major advantage of the capillary rheometer is that the flow properties of fluids can be characterized under high shear conditions (up to 10^6 s^{-1}) and process relevant temperatures (up to 400°C). Another advantage is that the capillary flow is closed and has no free surface so that edge effects, solvent evaporation and other problems that trouble the rotational rheometers can be avoided.

1.4 Rheology of Suspensions

The flow behavior of colloidal dispersions is controlled by the balance between hydrodynamic and thermodynamic interactions as well as Brownian particle motion. Thermodynamic interactions mainly include electrostatic and steric repulsion and van der Waals and depletion attraction. The relative importance of individual forces can be assessed on the basis of dimensionless groups which can be used to scale rheological experiments. In this section we first consider dispersions of Brownian hard sphere particles and elucidate the effect of particle volume fraction, size and shape of particles on dispersion rheology. Then, we take into account the effect of repulsion and attractive interactions on the microstructure of suspensions and its corresponding rheological response. Special attention will be paid to the rheological behavior of concentrated colloidal dispersions.

1.4.1 Hard spheres

Hard-sphere dispersions are idealized model systems where no particle–particle interactions are present unless these particles come into contact. In that sense, they represent the first step from ideal gases towards real fluids. Even such simple systems as these can show complex rheological behavior. The parameters controlling dispersion rheology will be discussed below.

1.4.1.1 Viscosity of suspensions of spheres in Newtonian media

Figure 1.6 demonstrates the general features of the shear stress dependence of suspension viscosity at different volume fractions, using the example of aqueous dispersions of 250 nm poly(styrene-ethylacrylate) (St/EA) particles[6]. It can be seen that viscosity increases with particle volume fraction ϕ and beyond about 30 % it becomes susceptible to shear stress. This can be understood considering the rest and flow induced microstructure of concentrated suspension. The shear rate at which the shear thinning behavior begins, depends on the balance between Brownian and hydrodynamic forces. Hence the Peclet-number Pe is a useful dimensionless quantity to expresses the relative importance of these two contributions:

[eq_026]

Equation 1.26

$$Pe = \frac{6\pi a^3 \eta}{k_B T} = \frac{a^2}{D_0}\dot{\gamma}$$

where a is the particle size, k_BT is the thermal energy and D_0 is the diffusion coefficient. The Peclet number is often called dimensionless shear rate, equivalently the dimensionless shear stress σ_r can be expressed as follows:

[eq_027]

Equation 1.27

$$\sigma_r = \frac{a^3 \sigma}{k_B T}$$

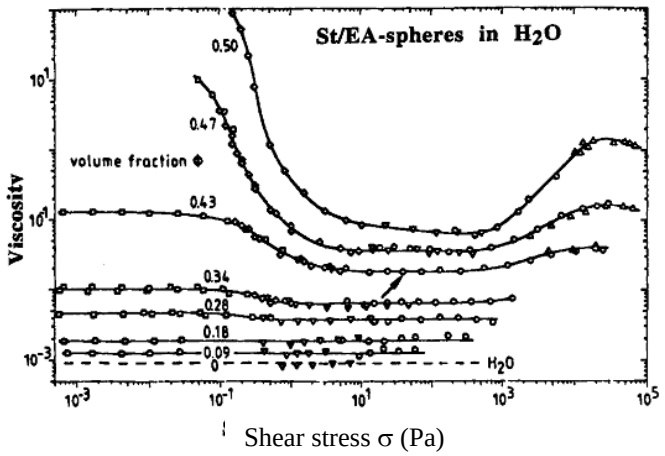

[Fig_006]

Figure 1.6 Viscosity as a function of shear stress σ for aqueous dispersions of 250 nm poly(styrene-ethylacrylate) at different particle volume fractions in the range ϕ = 0 – 0.5, as reported by Laun[6]

At low-shear rates the Brownian motion dominates (Pe < 1) and the rest-state structure remains undisturbed resulting in Newtonian behaviour of the concentrated dispersion. Thus the viscosity in this low-shear Newtonian regime equals the zero-shear viscosity η_0. Increasing the shear rate or correspondingly shear stress above a critical magnitude (Pe>1) the imposed velocity gradient induces an orientation of the particles resulting in gradually decreasing viscosity with

increasing shear rate. This is so called shear thinning regime. When the maximum amount of shear ordering is reached viscosity attains its minimum value η_∞ and becomes again independent of the shear rate (or shear stress). This region of the flow curve corresponds to the second Newtonian plateau. Further increase of the shear rate can induce viscosity increase, i.e. shear thickening behaviour, especially with concentrated suspensions.

An important clue to the understanding of the non-Newtonian behaviour of suspensions is the effect of particle concentration on suspension viscosity. Particles dispersed in a flowing liquid disturb the flow field giving rise to extra energy dissipation. The classical model of Einstein[7,8] for infinitely dilute, non-interacting hard spheres showed that single particles increase the viscosity of the dispersion medium as a linear function of the volume fraction ϕ, according to the equation:

[eq_028]

Equation 1.28

$$\eta_r \equiv \frac{\eta}{\eta_s} = (1 + 2.5\phi)$$

where η is the suspension viscosity, η_s is the viscosity of the suspension medium and η_r is the relative viscosity. The Einstein equation applies to $\phi < 0.01$, assuring that the flow around a particle does not influence the velocity field of any other particle. At higher particle concentration the hydrodynamic interactions between particles become important and higher-order terms in ϕ have to be considered. The effect of two-sphere hydrodynamic interactions on the suspension viscosity was calculated by Batchelor[9]:

[eq_029]

Equation 1.29

$$\eta_r = 1 + 2.5\phi + 6.2\phi^2$$

This equation is validated to $\phi < 0.1$. For higher particle concentrations multi-particle interactions become imperative and it is difficult to analyze theoretically. Numerous of phenomenological equations have been proposed to correlate viscosity of concentrated dispersions to the particle volume fraction. Krieger and Dougherty[10] proposed a semi-empirical equation for the concentration dependence of the viscosity:

[eq_030]

Equation 1.30

$$\eta_r = \left(1 - \frac{\phi}{\phi_{\max}}\right)^{-2.5\phi_{\max}}$$

where ϕ_{max} is the maximum packing fraction or the volume fraction at which the zero shear viscosity diverges. This equation reduces to the Einstein relation (Equation 1.28) at low particle concentration. Approaching the maximum volume fraction ϕ_{max} the particle packing density is such that the dispersion flow is impossible and $\eta_r \to \infty$. Quemada[11] suggested another phenomenological model to predict the $\eta_r(\phi)$ dependence:

[eq_031]

Equation 1.31

$$\eta_r = \left(1 - \frac{\phi}{\phi_{\max}}\right)^{-2}$$

The volume fraction dependence of relative viscosity, according to the models described above is shown in Figure 1.7

The absolute value for the maximum packing fraction ϕ_{max} is determined by the packing geometry which depends on the particle shape and particle size distribution but not on particle size. The volume fraction at maximum packing has been calculated by theoretical models and different ϕ_{max} values have been found depending on the type of packing. The ϕ_{max} value for hard spheres is often taken as 0.64[12], which is the value associated with random close packing. However, experiments of hard sphere dispersions have shown that zero-shear viscosity diverges at the volume fraction of the colloidal glass transition ϕ_g[13,14]. Colloidal glass transition is associated with the glass transition of ordinary glasses which occurs at a certain temperature bellow which the molecular mobility vanishes. Similar phenomenon is observed in colloidal dispersions. Above a critical particle concentration particle diffusion is restricted to small “cages” formed by the nearest neighbours, correspondingly the long-time self-diffusion coefficient decreases to zero and the viscosity diverges according to the generalized Stokes-Einstein relation:

[eq_032]

Equation 1.32

$$D = \frac{k_B T}{6\pi\eta(\phi)a}$$

The colloidal glass transition volume fraction ϕ_g of monodispersed hard sphere suspension is found to be 0.58[15,16].

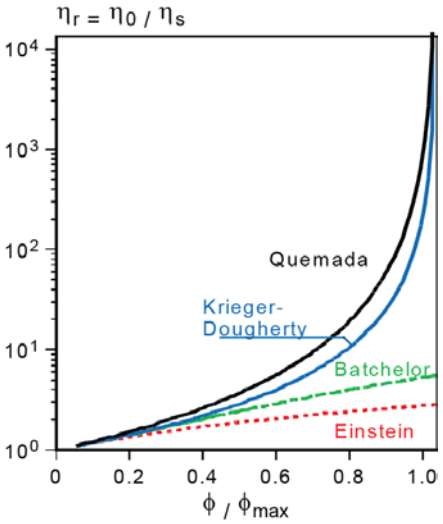

[Fig_007]

Figure 1.7 Schematic reprezantation of the volume fraction dependence of relative viscosity η_r according to the Einstein -, Batchelor -, Krieger-Dougherty - and Quemada model

It should be mentioned, that the Krieger-Dougherty relation describes rather well the volume fraction dependence of the limiting high-shear viscosity[17] but the maximum packing fraction ϕ_{max} have different values at low and high shear rates. An increase of the shear rate causes particle to align in the flow direction and determines more efficient packing than the random close packed structure at rest.

The normalized zero-shear viscosity as well as the limiting high-shear viscosity of hard sphere dispersions do not depend on the particle size and solely change with particle volume fraction. On the other hand, the particle size influences the shear viscosity in the shear-thinning region. This is due to the enhanced contribution of hydrodynamic interactions to the viscous dissipation, which increases with decreasing particle size because of the larger particle surface area and smaller interparticle separation at constant volume fraction. Since the shear thinning region occurs around a characteristic Peclet-number Pe ≈1, variation of particle size results in a

shift of the viscosity/shear rate curve on the $\dot{\gamma}$-axis with particle radius squared. Hence a plot of η_r as a function of Peclet number or the dimensionless shear stress σ_r should superimpose for hard sphere colloids of different particle size at given ϕ. This is illustrated in Fig (Figure 1.8) using the example of poly(methylmethacrylate) spheres of different size, dispersed in silicone oil[18].

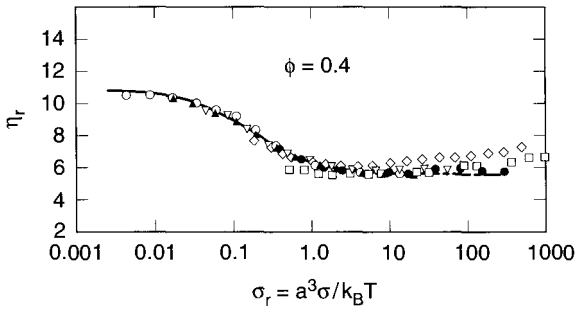

[Fig_008]

Figure 1.8 Relative viscosity η_r as a function of dimensionless shear stress σ_r for sterically stabilized poly(methylmethacrylate) particles of different size: 85, 141, 204 and 310 nm dispersed in silicon oil[18]

1.4.1.2 Non-spherical particles

Particles can deviate from the spherical form by either being axisymmetric or by having irregular shape. Typically particles are approximated by prolate or oblate spheroids (see Figure 1.9) with a specified axis ratio r_p:

[eq_033]

Equation 1.33

$$r_p = \frac{b}{a}$$

where b corresponds to the length of the particle along its axis of symmetry and a to its length perpendicular to this axis. Some examples of spheroids are shown in Figure 1.9. Rheology of suspensions of axisymmetric particles is greatly influenced by particle orientation with respect to the flow. Orientation of the spheroids in flowing suspensions is governed by the balance between hydrodynamic forces which tend to align particle with flow and the Brownian motion which tend

to randomize the orientation. The relative importance of each is given by a rotational Peclet number Pe_{rot}:

[eq_034]

Equation 1.34

$$Pe_{rot} = \tau_{rot}\dot{\gamma}$$

For disk-like particles with radius a, the rotational relaxation time τ_{rot} is:

[eq_035]

Equation 1.35

$$\tau_{rot}^{-1} = \frac{3kT}{32\eta_s a^3}$$

and for rod-like particles with length 2b such that r_p>>1:

[eq_036]

Equation 1.36

$$\tau_{rot}^{-1} = \frac{3kT(\ln 2r_p - 0.5)}{8\pi\eta_s b^3}$$

Consequently, at low shear rates for small particles and low fluid viscosity $Pe_{rot}\rightarrow 0$ and the randomizing effect of Brownian motion dominates. For $Pe_{rot} > 1$ the hydrodynamic forces become enough strong to align the particles with the flow and the suspension show a considerable shear thinning behavior.

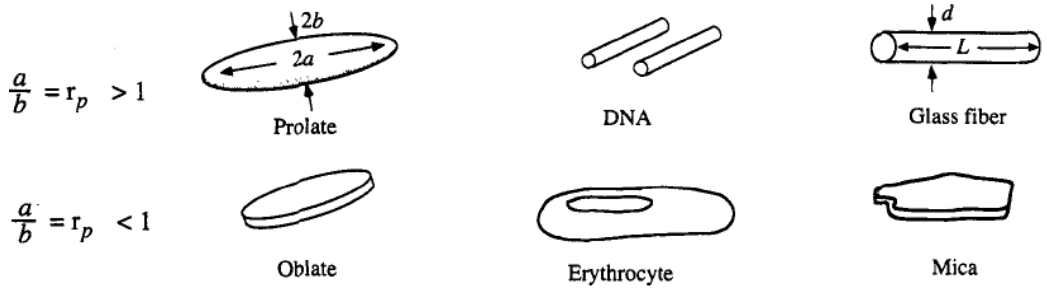

[Fig_009]

Figure 1.9 Prolate or oblate shaped particles and correspondent examples of typical particles (taken from Macosko "Rheology Principles, Measurements, and Applications"[2])

Figure 1.10a–b shows numerical results of intrinsic viscosity [η] as a function of Pe_{rot} for dilute suspensions of disk- and rod-like particles at different aspect ratios[19]. Note that the intrinsic viscosity [η] for suspensions is a dimensionless quantity defined as:

[eq_037]

Equation 1.37

$$[\eta] = \lim_{\phi \to 0} \frac{\eta - \eta_s}{\phi \eta_s}$$

It can be seen from Figure 1.10a–b that the zero-shear intrinsic viscosity increases with increasing the aspect ratio r_p, which is due to the effective enlargement of the volume inaccessible for other particles. Elongated particles in highly diluted suspensions can rotate freely about its balance point and thus disturb the flow as a sphere with diameter corresponding to the long dimension of a spheroid.

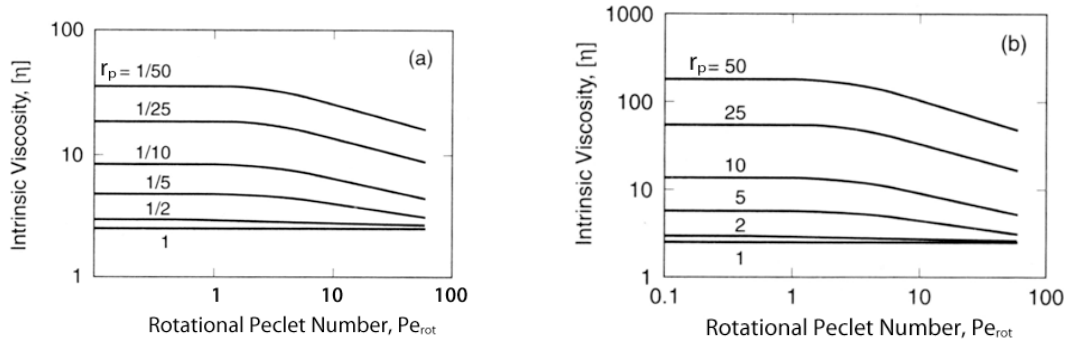

[Fig_010]

Figure 1.10a–b Intrinsic viscosity [η] as a function of rotational Peclet number Pe_{rot}, calculated for diluted suspensions of **a** disc- and **b** rod-like particles of various aspect ratios[19]

Particle asymmetry also has a strong effect on the maximum packing fraction and thus on the concentration dependence of viscosity. Since the effective volume of elongated particles increase strongly with increasing the aspect ratio, particle-particle interactions should be expected at lower volume fraction than for sphere suspension with the same phase volume. Although axisymmetric particles could be packed more closely than spheres, the divergence of the zero

shear viscosity occurs at lower volume fraction and decrease with increasing the aspect ratio [Fig from Giesekus 1983 and Clarke 1967,].

1.4.2 Influence of Colloidal Interactions on Rheology

1.4.2.1 Repulsive Particles

So far we considered suspensions of hard spheres for which the colloidal interactions did not play a role. In practice, dispersions are stabilized by repulsive surface forces in order to prevent aggregation. Colloidal interactions like electrostatic or steric repulsion keep particles far enough apart that they can not be attracted by the short-range van der Waals attraction force. Increasing the range of repulsion forces the effective particle radius a_{eff} increases and hence the excluded volume which is inaccessible to other particles. The effective volume fraction of the dispersion ϕ_{eff} can be expressed as follows:

[eq_038]

Equation 1.38

$$\phi_{eff} = \phi\left(\frac{a_{eff}}{a}\right)^3$$

Many rheological features are analogous to those of hard sphere dispersions and can be quantitatively described by mapping the real system onto a hard sphere system with $\phi = \phi_{eff}$. The effective increase of the volume of charged particles causes an increase of the zero-shear viscosity as well as formation of microcrystalline phases at lower particle volume fractions than in the case of hard spheres.

The DLVO-theory provides a good description for the interactions among electrostatically stabilized colloidal particles (see chapter 2 in volume 1 of “Product Design and Enginiring”[20]). The strength of the repulsion is given by the surface charge or surface potential and the range of interaction by the so-called Debye length κ^{-1}, which is inversely proportional to the square-root of the ion concentration in the liquid phase. Since the effective volume fraction ϕ_{eff} increases with increasing Debye length κ^{-1}, the viscosity of charge-stabilized dispersions strongly depends on particle surface charge and ionic strength of the dispersion medium and diverges at lower volume fraction than predicted for hard spheres. Horn et al. measured the concentration dependence of the zero-shear viscosity for monodispersed charged polystyrene latices (PS) at

range of ionic strengths and particle sizes[21]. Figure 1.11a shows that the relative zero-shear viscosity $\eta_{0,r} = \eta_0/\eta_s$ diverges at volume fraction $\phi_{max,exp}$ well below the one typical for hard spheres and this experimental maximum volume fraction $\phi_{max,exp}$ decreases with decreasing the ionic strength of the system. Particle size is also an important parameter which influences ϕ_{eff}. As evident from Equation 1.38, decreasing the particle radius a, at a constant volume fraction ϕ and constant ionic strength, corresponds to an increase of ϕ_{eff} and thus phase transition at lower particle concentration. It has been observed experimentally[21] that, for smaller particles, the zero-shear viscosity diverges at lower particle volume fraction $\phi_{max,exp}$, keeping all other conditions the same. The effect of particle size and ionic strength on the volume fraction dependence of dispersion viscosity can be reduced to a universal master curve by rescaling the volume fraction by $\phi/\phi_{max,\,exp}$ (Figure 1.11b). Furthermore, the Quemada (Equation 1.31) and Krieger-Dougherty (Equation 1.30) equations developed for hard sphere dispersions provide a good description of the low shear viscosity data for the electrostatically interacting systems, as can be seen in Figure 1.11b.

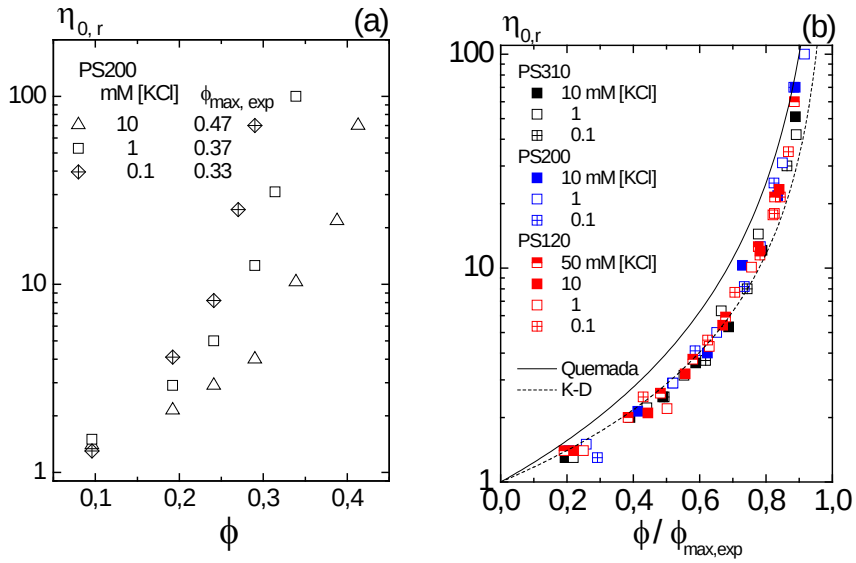

[Fig_011]

Figure 1.11a–b **a** Relative zero-shear viscosity $\eta_{0,r}$ versus particle volume fraction ϕ for monodisperse polystyrene particles (PS200) of 200 nm in diameter dispersed in water at different potassium chloride concentration [KCl] **b** Master curve for all the data including the polystyrene dispersions at different salt concentration and particle size: 120, 200, 310 nm [21]

Electrostatic interactions have a strong impact on the microstructure or phase behaviour of colloidal dispersions and hence on their flow properties. Figure 1.12 demonstrates the relative

viscosity as a function of shear rate at various concentrations of electrostatically stabilized polystyrene/acrylate dispersion. It can be seen that at low volume fractions the dispersion is in liquid state and a low-shear plateau is observed for the viscosity. Increasing the particle volume fraction, the onset of shear thinning shifts to lower shear rates and the degree of shear thinning increases. The hysteresis of the flow curve at ϕ=0.44 indicates thixotropic behaviour, which is due to the shear-induced dissociation and consequent recovery of sample structure. The sample structure at this particle concentration is associated with coexisting liquid and gel-like domains. This is the transition two phase region before the gel-like state. For particle volume fractions above $\phi_{max,\,exp}$ dispersions are in the crystalline or gel like state and show shear thinning behaviour in the whole shear rate range investigated. On the other hand the thixotropy vanishes due to the dense particle packing.

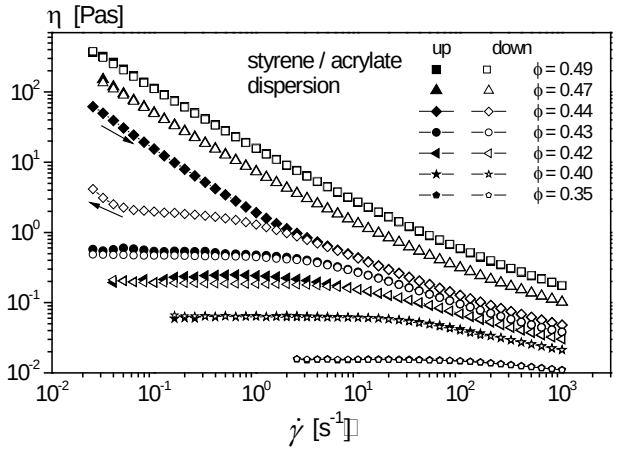

[Fig_012]

Figure 1.12 Viscosity as a function of increasing (down) and decreasing (up) shear rate for polystyrene/acrylate dispersion measured at various particle volume fractions. The downward arrow indicates the viscosity measurement with increasing the shear rate and the upward arrow indicates the consequent measurement at gradually decreasing shear rates.

At sufficiently high shear rates hydrodynamic interactions become dominant and can overcome repulsion forces so that particles approach each other closer and a_{eff} decreases. Charge stabilized dispersions show a strong shear thinning behavior until viscosity is close to that expected for hard spheres, i.e. independent of particle size and ionic strength. This is true for the high shear viscosity η_∞ as well as the high frequency viscosityη'_∞. Note that these quantities correspond to different microstructures and η_∞ is always larger than η'_∞. The Cox-Merz rule states:

[eq_039]

Equation 1.39

$$\eta(\dot{\gamma}) = \left|\eta^*(\omega)\right| \text{ for } \dot{\gamma} = \omega$$

However, it is valid only at low shear rates and/or low particle loading.

The linear viscoelastic properties of electrostatically stabilized suspensions drastically change from predominantly viscous to highly elastic at the liquid/crystalline phase transition. This is illustrated in Figure 1.13 , showing the frequency dependence of the elastic modulus G′ and viscous modulus G″ for three different particle volume fractions. At intermediate volume fractions the dispersion shows a viscoelastic behavior described by the Maxwell model, while in the gel state the G′ and G″ become frequency independent. The G′ plateau modulus is assigned as G_0 and increases by orders of magnitude within a narrow concentration range. The dependence of G_0 on ϕ can be described by the scaling law:

[eq_040]

Equation 1.40

$$G_0 = k\phi^n$$

where k is a prefactor and n is an exponent corresponding to the slope of the line in log-log plots of G_0 versus ϕ. The power-law exponent n depends strongly on the range of repulsion i.e. on the Debye-Huckel constant κ^{-1}.

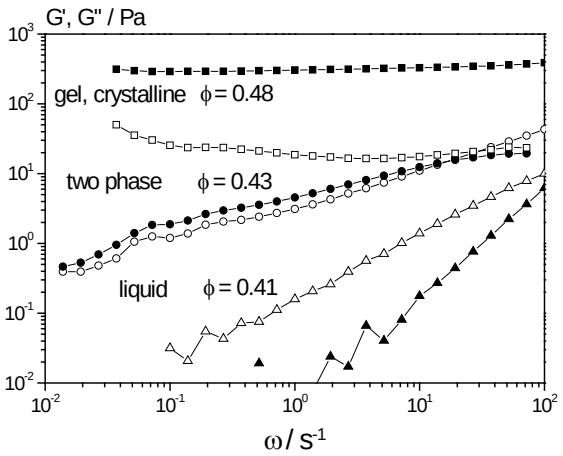

[Fig_013]

Figure 1.13 G′ and G″ as a function of angular frequency ω for a concentrated electrostatically stabilized dispersion at volume fractions around the phase transition region. The field symbols denote G′ while the open symbols G″

Let us now consider the rheology of sterically stabilized dispersions. Particle repulsion in sterically stabilized dispersions results from the interactions between polymer chains or surfactant molecules adsorbed or grafted onto the particle surface. The formation of hairy surface layer gives rise to an increase in the hydrodynamic particle radius and dispersions zero-shear viscosity, in a similar way as in the case of charged particles. Hence, the rheological behavior of such systems is similar to that of hard spheres with a_{eff}= a+L. Decreasing the particle radius a the thickness of the stabilizing layer L can contributes significantly to the effective volume ϕ_{eff}.and thus give rise to the viscosity. When using polyelectrolytes or ionic stabilizers with weak-type functional acid groups, the thickness of the stabilizer layer L depends on the ionic strength and pH of the dispersion medium, which determine the degree of dissociation and range of electrostatic interactions among the functional acid groups. The steric repulsion provided by this surface layer, which is activated and tuned by short range electrostatic interactions is called electrosteric stabilization and is the dominating mechanism for stabilization of commercial polymer dispersions. As was the case for charged particles, electrosterically stabilized dispersions show universal scaling independent of ionic strength, pH or core particle size, but here the data have to be re-scaled and plotted versus ϕ_{eff} not only for the zero-shear viscosity η_0 but also for the high shear viscosity η_∞ and high frequency viscosity η'_∞. However the hairy particles show the same η'_∞ as predicted for hard sphere dispersions up to ϕ_{eff} = 0.5. Beyond this effective volume fraction strong deviations are observed due to the permeability and interpenetration of the stabilizing layers[22].

1.4.2.2 Attractive Particles

Attractive particle interaction either result in large compact aggregates, which rapidly phase separate, or in loose aggregates with fractal structure. Only the latter case is relevant for the rheology of colloidal dispersions. Loose aggregates immobilize water leading to larger effective volume fraction ϕ_{eff} and thus to an increase in the zero-shear viscosity. When the shear rate is increased the flocs gradually break-down resulting in a strong shear thinning. At high enough shear rates the aggregates breack-up into primary particles or cannot break-down further and the viscosity attains its minimum value, a pseudo-Newtonian region is reached. Aggregate break-up

in dilute dispersions can be estimated by the balance between hydrodynamic forces $F_H = 6\pi\eta_s a^2\dot{\gamma}$ and the van der Waals force $F_{vdW} = aA_H/12h^2$ (where A_H is the Hamaker constant and h interparticle separation distance). Hence, in the colloidal domain (a < 1μm) very large shear rates are required to break-up the aggregates into primary particles.

The fractal structure of aggregates is characterized by the fractal dimension D_f which describes the mass density of the flocs and is controlled by the aggregation mechanism. Note the lower the D_f value, more open the aggregate structure becomes. Reaction limited- and flow induced aggregation lead to denser structures, while diffusion limited aggregation results in low D_f values, as confirmed by computer simulation and scattering experiments[23,24,25]. Above a critical volume fraction fractal aggregates can interconnect forming sample-spanning network, which results in a highly elastic gel-like behavior (G′ > G″) and an apparent yield stress. The rest structure usually ruptures at very small stress levels and viscosity progressively decreases with increasing applied stress. The shear induced break-down and recovery of flocs require a finite amount of time resulting in a thixotropic behavior. Recovery of aggregate structure is forced by the Brownian motion and attractive forces and thus the rate of thixotropic recovery depends on particle size.

Depending on the magnitude and balance of interaction forces as well as the presence of additives, different flocculation mechanisms can be recognized:

- *Flocculation of charged particles* can be caused by increasing the ionic strength and or lowering the surface charge. Particles can then aggregate in the primary or the secondary minimum of the potential energy curve. The latter gives rise to fairly week aggregates and a shear force can easily separate the particles again.
- *Flocculation of strerically stabilized particles* depends on the thickness of stabilizing layer. When it is not sufficiently thick to screen the van der Waals attraction particles may coagulate in a shallow primary minimum.
- *Depletion flocculation* results when adding non-adsorbing polymers, free to move in the dispersion medium. This phenomenon may be understood by considering two particles approaching one another in a solution of free polymer. As the gap between them becomes too small to contain the polymer molecules, the local osmotic conditions will cause the pure dispersion medium to flow out of the gap between particles leading to weak attraction. Attractive interactions in this case are easily tunable by size and concentration of added polymer. Depletion strongly affects phase behavior of concentrated dispersions resulting in a strong increase in low-shear viscosity and the occurrence of an apparent yield stress. Formation of weak aggregates by depletion aggregation can also shift the colloidal

glass transition ϕ_g to significantly higher values and this so-called re-entry phenomenon can be used to fluidize highly concentrated dispersions.

- *Bridging flocculation* occurs when dissolving high-molecular polymers with strong affinity to particle surface which attach to at least two particles. Strong bridging-flocculated gels maybe formed at high particle volume fraction.
- *Flocculation by capillary forces*; the addition of small amounts of a secondary fluid, immiscible with the continuous phase of the suspension, causes agglomeration due to the capillary bridges and creates particle networks even at low particle volume fraction.

Investigations on the rheology of strongly flocculated gels are difficult, because of the poor reproducibility of sample preparation, sensitivity to shear history and preparation conditions. On the other hand, weak or reversible flocculation allows for breakup and re-formation of aggregates due to thermal forces and the structure achieves thermodynamic equilibrium.

1.4.2.2.1 Rheology of Weakly Flocculated Gels

To demonstrate some features of the rheology of weakly flocculated gels let us consider the results of the investigations of depletion flocculated suspensions and the thermoreversible gelation of sterically interacting particle suspensions. Figure 1.14 shows the shear rate dependence of the relative viscosity of colloidal dispersions of octadecyl grafted silica spheres in benzene ($\phi = 0.367$) at several temperatures[26]. Decreasing the temperature below the theta temperature (316 K) weak aggregates are formed, leading to increase in viscosity and shear thinning behavior.

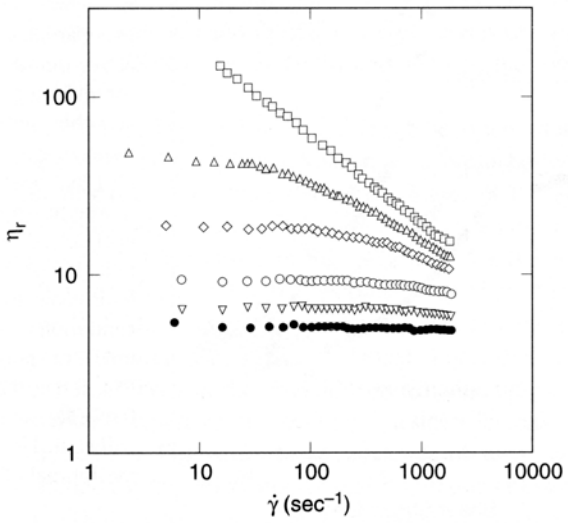

[Fig_014]

Figure 1.14 Relative shear rate versus shear rate for dispersion of octadecyl grafted silica spheres in benzene (ϕ=0.367) at several temperatures: 317.28 K, 308.13 K 306.20 K, 304.17 K, 303.16 K and 302.16 K (from bottom to top)[26]

Buscall et al.[27] studied sterically stabilized acrylic copolymer particles dispersed in "white spirit" (mixture of high-boiling hydrocarbons). Adding non-adsorbing polyisobutylene above the critical free polymer concentration for depletion flocculation causes a dramatic increase in viscosity with increasing polymer concentration (Figure 1.15).

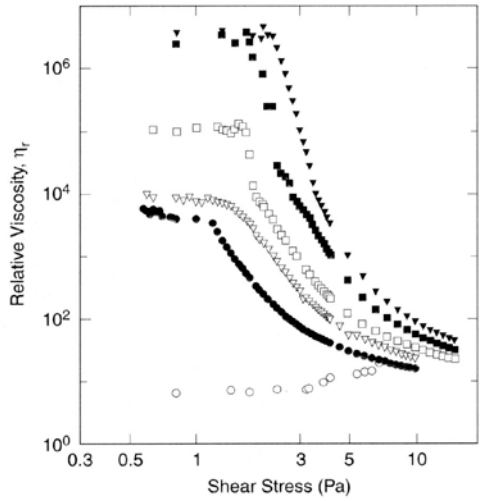

[Fig_015]

Figure 1.15 Shear stress versus relative viscosity for dispersion of acrylic copolymer particles (a = 157 nm) grafted with hydroxystearic acid- polymethylmethacrylat and dispersed in "white spirit"at volume fraction ϕ = 0.4 with added polyisobutene (M_w = 411000 g/mol) of different concentrations in weight per volume: 0.1 %, 0.4 %, 0.5 %, 0.6 %, 0.85 %, 1 % (from bottom to top) [27]

Weakly flocculated systems are also characterized by a yield stress. Tadros et al.[28] investigated depletion flocculated aqueous polystyrene dispersions containing "free" polyethylene oxide (PEO) chains. It was found that the yield stress σ_y increases linearly with increasing PEO concentration ϕ_p and the slope of this linear dependence increases with increasing the particle volume fraction ϕ (Figure 1.16). The following scaling relations can be applied to describe the particle volume fraction dependency of yield stress σ_y:

[eq_041]

Equation 1.41

$$\sigma_y \sim \phi^p$$

where the power-law exponent p depends on the fractal dimension and is around 3 according to experimental investigations, while numerical simulations report higher values: 3.5 - 4.4, depending whether the aggregation is slow or rapid (Ref).

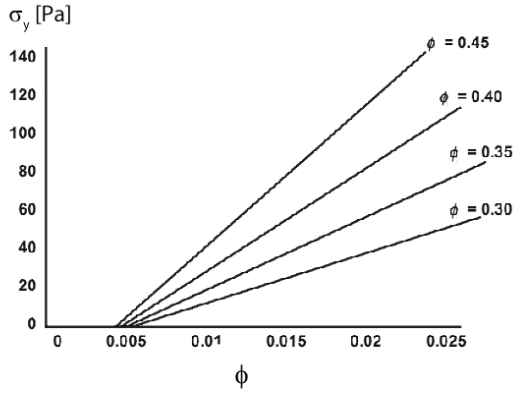

[Fig_016]

Figure 1.16 Yield stress σ_y versus free polymer (PEO, M_w = 20000) volume fraction ϕ_p for polystyrene dispersion at several particle volume fractions ϕ[28]

Viscoelastic measurements provide a better understanding of the structure of flocculated dispersions. Figure 1.17 shows the elastic modulus G′of the depletion-flocculated aqueous polystyrene dispersions (a=77.5) as a function of the free polymer (PEO) volume fraction ϕ_p at several particle volume fractions. Above the critical free polymer concentration G′ increases with increasing ϕ_p sice the aggregates grow. G′ reaches a plateau value as soon as a sample-spanning network is formed. Furthermore in can be seen that any given ϕ_p the elastic modulus G′increase with increasing particle volume fraction. Furthermore in Figure 1.17 can be seen that at any given ϕ_p, the elastic modulus G′increases with increasing particle volume fraction.

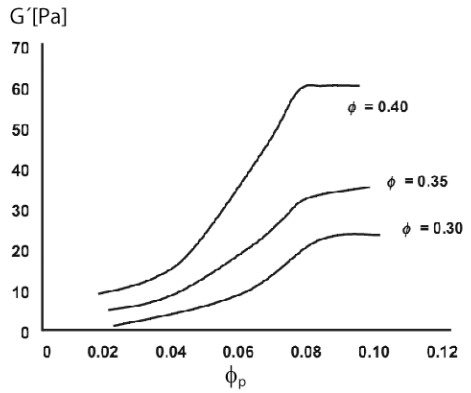

[Fig_017]

Figure 1.17 The elastic modulus G′ versus free polymer (PEO, M_w = 20000) volume fraction ϕ_p for polystyrene dispersion (a=77.5) at three different particle volume fraction ϕ[28].

1.4.2.2.2 Rheology of Strongly Flocculated Gels

As strongly aggregated suspensions are classified systems in which particles are captured in deep primary or secondary minimum with $(-\Psi_{min}/k_BT) > 20$ (where Ψ_{min} is the minimum of interaction potential). Such systems are not at equilibrium and hence difficult to investigate experimentally. Nevertheless several studies[29,30,31] examined the rheological properties of strongly flocculated gels and found some typical trends for these materials. Strongly flocculated gels are highly elastic (G′ >> G″) at small amplitudes and have extremely limited range of viscoelastic response. Above a critical amplitude γ_y the elastic modulus G′ rapidly decreases since the flocculated structure break down with applied shear. For strongly flocculated systems γ_c is much lower than for stable dispersions with repulsive interactions or for polymer melts and solutions. The elastic modulus G′ of strongly flocculated gels, measured in the linear viscoelastic range is always frequency independent, indicating inflexible gel like structure. Furthermore, G′ is independent of particle size but strongly depends on the particle volume fraction ϕ. Scaling laws can be applied to describe this dependence:

[eq_042]

Equation 1.42

$$G' \sim \phi^{\alpha}$$

where the exponent α varies between 2 and 6 depending on the aggregation conditions. If aggregation is slow (reaction limited) dense structures are formed and gel formation sets in a higher particle volume fraction, correspondingly α is high. As an illustration, Figure 1.18 shows a log-log plot of the variation of G′ with particle volume fraction ϕ for polystyrene particles in water flocculated by adding salt (NaCl)[32], well above the critical coagulation concentration (CCC). The exponent α found here is equal to 6, indicating dense floc structure.

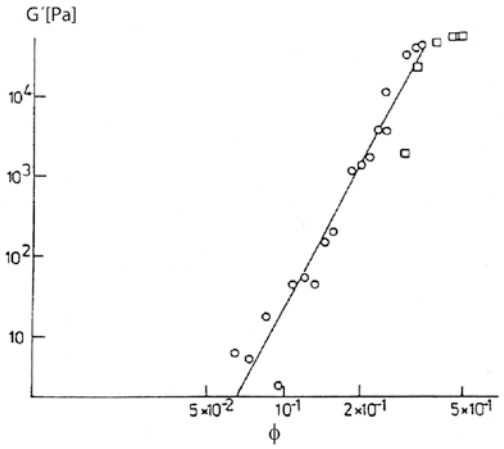

[Fig_018]

Figure 1.18 Elastic modulus G′ versus particle volume fraction ϕ for polystyrene particles in water flocculated by adding 0.2 mol/l NaCl[32]

Strongly flocculated dispersions are very sensitive to shear and are characterized by a yield stress. The yield stress σ_y of an aggregated dispersion can be related to the adhesion force F_{adh} between two particles[17]:

[eq_043]

Equation 1.43

$$\sigma_y = \frac{F_{adh}}{a^2} f(\phi)$$

The term F_{adh}/a^2 is the stress per particle and the function $f(\phi)$ can be approximated as the number of binary contacts, i.e. $f(\phi) = \phi^2$. For dense systems more elaborate models predicting $f(\phi)$ are available. The adhesion force is given by the derivative of the interaction potential with respect to the separation distance, which can be estimated from the DLVO-theory. Experimental studies[31,32] have revealed a simple scaling for the yield stress of strongly flocculated particulate gels:

[eq_044]

Equation 1.44

$$\sigma_y \sim \frac{\phi^3}{a^2}$$

1.4.2.2.3 Capillary Forces in Suspension Rheology

Recently, Koos and Willenbacher[33] reported that reversible flocculation by capillary forces can dramatically change the rheological properties of dispersions. The addition of small amounts of a secondary fluid, immiscible with the continuous phase of the suspension, causes flocculation due to the capillary liquid bridges between particles and formation of sample-spanning network structure thus leading to a transition from predominantly viscous to gel like behavior. This phenomenon is observed for variety of different fluid/particle systems, independent of whether the primary liquid or the secondary immiscible liquid preferentially wet the solid particles. When the secondary fluid is the fluid creating isolated capillary bridges between particles the observed gel-like state is termed the "pendular" state, analogous to the pendular state in wet granular media (see chapter 2, in volume 1 of "Product Design and Enginiring"[20]). Even if the second, immiscible fluid does not preferentially wet the solid particles it can still attach to the particles and cause agglomeration due to the strong capillary force from the bulk wetting fluid. This state is analogous to the capillary state in wet granular media. Figure 1.19 shows the effect of the fraction of wetting liquid on the yield stress for both pendular and capillary state. The increase in yield stress is greatest in the capillary state for the aqueous polyvinyl chloride (PVC) dispersion with diisononyl phthalate (DINP) as a secondary fluid. In contrast, the maximum in the yield stress for the dispersion of Hematite particles in DINP is in the pendular state where water is the secondary fluid.

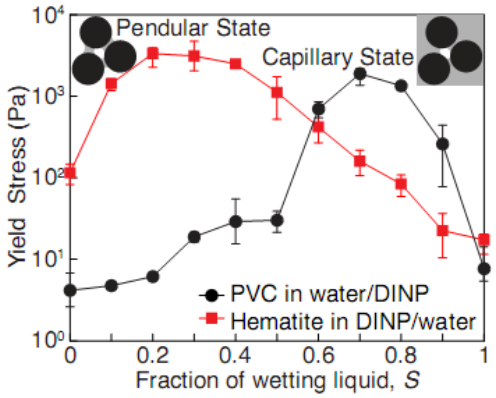

[Fig_019]

Figure 1.19 Yield stress versus fraction of wetting liquid S. For the aqueous PVC dispersion with addition of DINP the yield stress show a maximum in the capillary state. Adding water to the suspension of Hematite particles in DINP the yield stress shows a maximum in the pendular state

Small amplitude oscillatory shear measurements of suspension in the capillary state clearly demonstrate the transition between the weakly elastic, predominantly viscous to highly elastic, gel-like behavior with increasing the amount of secondary fluid. Figure 1.20 shows the frequency dependence of the complex shear modulus G* for hydrophobically modified calcium carbonate (Socal) particles suspended in a silicone oil and added different amounts of water as a secondary fluid. Without the secondary fluid the magnitude of the complex shear modulus |G*| increases with increasing frequency, whereas addition only 0.2% wt. of water, the complex shear modulus G* becomes frequency independent. Note that this transition occurs at particle volume fraction as low as about 10%.

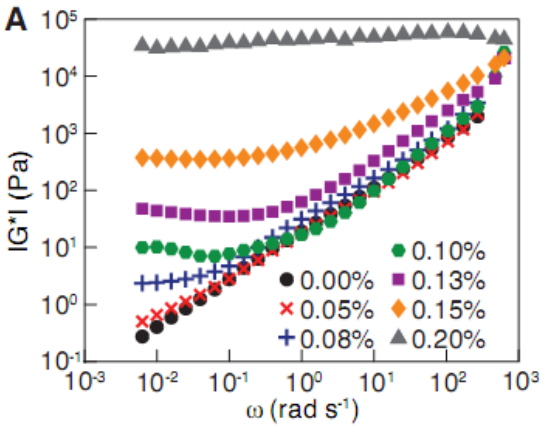

[Fig_020]

Figure 1.20 Magnitude of complex shear modulus |G*| versus frequency ω for socal particles (a = 800 nm, ϕ = 0.173) dispersed in a silicone oil adding various amounts of water.

Compared to the van der Waals force the force due to bridges between two particles in a contact is much stronger and is given by:

[eq_045]

Equation 1.45

$$F_c = 2\pi a \Gamma \cos\theta$$

where Γ ist he surface tension and θ is the wetting angle The magnitude of the capillary force depends also on the interaparticle separation and decreases with decreasing the particle volume fraction.

This phenomenon has important potential industrial applications. The addition of a second fluid to a suspension allows for avoiding sedimentation and keeps the mixture homogeneous

through the formation of sample-spanning network. Furthermore, capillary forces in suspensions can dramatically change the rheological properties of the system, which is a reversible process and can be adjusted by temperature or addition of surfactant. Another field of application is as precursor for porous ceramics or foams. A solid PVC foam has been already produced in laboratory conditions, using PVC particles ($\phi = 0.2$) dispersed in water and DINP as a secondary fluid[33].

1.4.2.2.4 Fluidization of Highly Concentrated Dispersions

Highly concentrated dispersions with particle volume fraction above the colloidal glass transition ϕ_g behave as gel-like materials with finite plateau modulus G_0. A classical method to shift the maximum packing fraction is by mixing of particles of different size (refer to section 1.4.3). However, in this section we will consider an alternative concept to fluidize dense colloidal dispersions, based on the so called re-entry glass transition in colloidal dispersions.

Theoretical[34,35,36]as well as experimental[37,38,39,40,41] results reveal that weak attractive interactions among particles, e.g. introduced by the depletion effect of non-adsorbing polymers, result in reversible particle clustering and thus leave space for long-range particle motion and macroscopic flow. Several investigations revealed that the low-shear viscosity of hard sphere-like colloidal dispersions exhibits a minimum as the concentration of added non-adsorbing polymer increases at particle volume fraction close to the hard sphere glass transition[42],[43].Eckert and Bartsch[39]**Fehler! Textmarke nicht definiert.**[41] studied the glass transition dynamics of hard sphere-like polystyrene microgel particles with depletion attractions by means of light scattering experiments (DLS). They showed that increasing the attraction strength the hard sphere glass transition shifts to higher volume fractions up to 70 %. At higher attraction strengths the hard sphere glass freeze again but into another type of glass state, termed attractive [44] or bonding-driven[45] glass. This phenomenon is called re-entry glass transition.

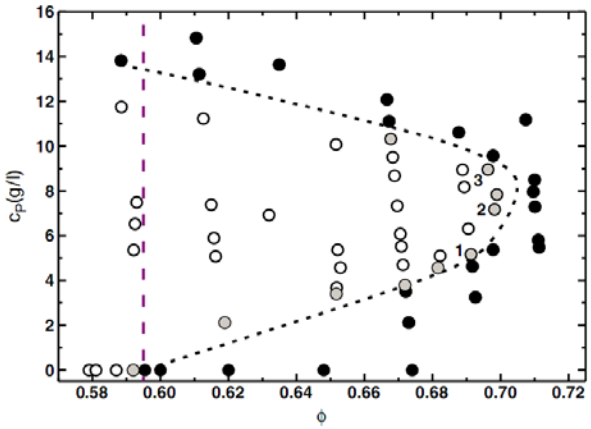

[Fig_021]

Figure 1.21 Re-entry phase diagram for binary polystyrene microgel colloidal dispersion with added liner polystyrene. The open symbols indicate samples in the fluid state, closed symbols represent the glass state, and shaded symbols denote the transition region. The dashed curve indicates the extrapolated location of the glass transition and the dashed vertical line shows the glass ransition of the microgel dispersion without free polymer.

Figure 1.21 shows the re-entry phase diagram of binary polystyrene microgel dispersion at different particle volume fractions as a function of added linear polystyrene with concentration c_p in g/l. The dashed vertical line indicates the glass transition line for the pure binary microgel mixture, while the dashed curve indicates the extrapolated location of the glass transition. The large re-entry region observed in the microscopic dynamics via DLS has been confirmed rheologically by Willenbacher et al.[46] using the same polystyrene microgel binary mixtures as Eckert and Bartsch[41]. In addition, Willenbacher et al[46] studied the re-entry phenomenon for the class of aqueous dispersions, using electrostatically stabilized hard sphere-like polystyrene-butylacrylate dispersion as a model system. The addition of non-adsorbing depletion agent (linear PEO) to the aqueous dispersion resulted in fluidization of the system up to $\phi \approx 0.644$. The change in the flow curves with concentration of added PEO (M_w = 10.000 g/mol) is shown in Figure 1.22a for particle volume fraction $\phi \approx 0.644$. A sharp drop in the low-shear viscosity is observed while the high-shear viscosity remains unaffected. The relative viscosity at constant low-shear rate plotted as a function of polymer concentration Figure 1.22b shows a clear viscosity minimum at 8 g/l PEO concentration. At even higher polymer concentrations the bonding-driven glass state begins to develop and the relative viscosity increases. Willenbacher et[46] al also demonstrated that low-shear viscosity can be reduced to the level of commercial dispersion with broad particle size distribution.

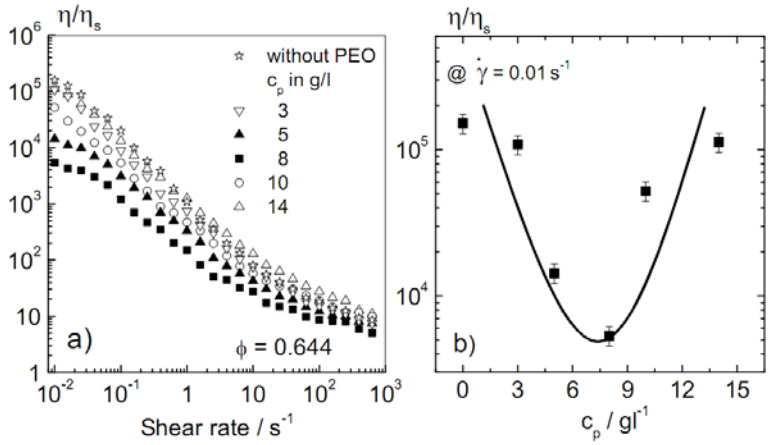

[Fig_022]

Figure 1.22a–b a Relative viscosity as a function of shear rate for an acrylate dispersion ($\phi \approx 0.644$) with different PEO (Mw = 10000 g/mol) concentration c_p in g/l, **b** relative low-shear viscosity (at $\dot{\gamma}=0.01\ s^{-1}$) versus the PEO concentration c_p[46]

1.4.3 Effect of Particle Size Distribution

Particle-size distribution has a strong impact on the rheology of highly concentrated (typically $\phi > 0.5$) dispersions of repulsively interacting particles. Viscosity can drop by more than an order of magnitude when suspensions with broad size distribution are compared to those with narrow size distribution at the same particle volume fraction. This is attributed to the more efficient packing of polydisperse spheres when the size ratio $\chi = a_{large}/a_{small}$ is large, since the voids between large particles can be filled with smaller particles. A theoretical treatment[47] assumed no interaction between small and large particles with size ratio $\chi > 10$, so that the small particles together with the solvent molecules behave as a fluid, and found that the viscosity of bimodal suspensions at a given total solids concentration is minimized at volume fraction of small particles ξ_s around 0.27. Experimental studies on hard-sphere like dispersions of non-Brownian glass beads[48] as well as for Brownian hard spheres[49] confirmed an optimum small particle volume fraction ξ_s of about 0.3 at which a viscosity is minimized. McGeary[50] extensively studied the geometric packing properties of multimodal suspensions of glass beads and showed that the most efficient particle packing can be achieved at critical size ratio χ=6.46, at which the small particles perfectly fit into the voids between the large ones. However, this simple geometrical packing argument is very unlikely, since for size ratio $\chi = 6.46$ and fraction of small particles $\xi_s = 0.25$, the number ratio of small to large particles $N_{small}/N_{large} \approx 90$[51], which means that the pores between large particles are much less than the number of small particles. Furthermore, experimental studies revealed that the phenomenon of viscosity reduction is still present even for size ratio χ much smaller than 6.5. Rodriguez et al[49] showed that for Brownian hard sphere dispersions with size ratio χ=1.7 viscosity goes through a minimum at ξ_s=0.35, but only at total particle loadings above ϕ=0.55. For suspensions of non-Brownian particles has been shown that viscosity reduction monotonically increases with increasing the size ratio χ and total particle volume fraction ϕ[48] (see Figure 1.23). Furthermore, note that bimodal size distribution can lead to ordered superlattice structures[52] or phase separation[53,54].

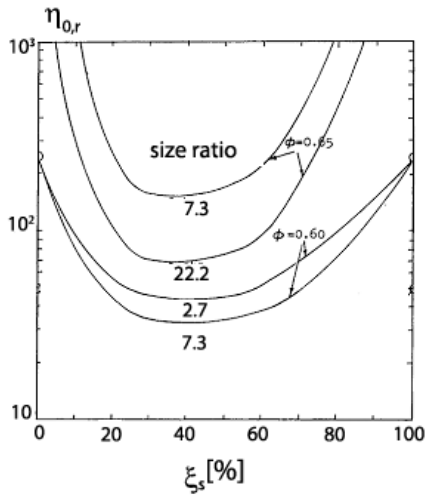

[Fig_023]

Figure 1.23 Calculated relative viscosity as a function of small particle volume fraction for a suspension of non-Brownian hard spheres at different size ratios. Adapted from Chong et al[48]

Experimental observations suggest that viscosity is the lower the larger the particle size ratio is, but this is no longer valid when colloidal interactions get significant. Then adding more and more small particles corresponds to an increase in the effective volume fraction ϕ_{eff} at constant particle loading ϕ, thus leading to a monotonic increase in viscosity. Figure 1.24 shows the effect of particle size ratio on the viscosity of hard sphere dispersion in comparison to colloidally interacting particles[51]. For this calculations the diameter of large particles is fixed to 800 nm, while the size of small particles is decreased, keeping the small particle volume fraction ξ_s=0.25 and total particle volume fraction ϕ = 0.6 constant. It can be seen that for hard sphere systems viscosity drops monotonically with increasing the size ratio. When colloidal interactions get relevant the effective volume ϕ_{eff} increases as the size of small particles decreases and thus viscosity goes through a minimum before increasing again. Typically, the viscosity minimum at constant volume fraction is observed for χ between 4 and 5. Note that the curves in Figure 1.24 have been calculated according to the generalized Quemada equation[55]:

[eq_046]

Equation 1.46

$$\eta = \tilde{\eta}\left(1-\frac{\phi}{\phi_{max}}\right)^{-\varepsilon}$$

where $\tilde{\eta}$ is a pre-factor which determine the viscosity level and depends on the shear arte, only[51]. The maximum packing fraction ϕ_{max} is fully defined by the particle size distribution[56] and the colloidal interactions are parameterized by the exponent $\varepsilon \geq 2$. The exponent ε is equal to 2 in the hard sphere limit and increases with decreasing the mean particle size. This is attributed to the fact that colloidal interactions among particles get more important as the mean particle separation diminishes and viscosity diverges at lower volume fractions than expected for hard spheres.

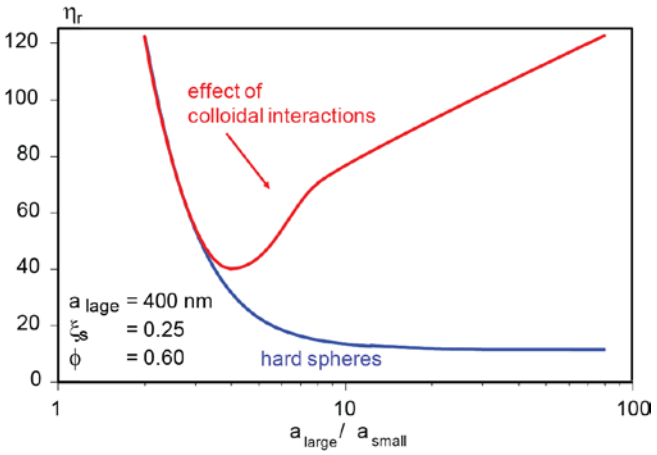

[Fig_024]

Figure 1.24 Viscosity as a function of particle size ratio calculated according to Equation 1.46 for large paricle raduis a_{large} = 400 nm, total particle concentration ϕ=0.6 and small particle volume fraction ξ_s=0.25. The blue curve shows the results for ε = 2, i.e. hard sphere dispersions and the red curve represents the results for ε as a function of average particle size. Adapted from Dames et al.[51]

1.4.4 Shear Thickening

Shear thickening describes the phenomenon of increasing viscosity with increasing shear rate or shear stress. This phenomenon has been observed for a wide variety of colloidal and non-colloidal particle suspensions. Shear thickening becomes important at high shear rates and occurs beyond a critical volume fraction (see Figure 1.6). The thickening effect increases with particle loading and depends on the particle size, particle size distribution shape and interactions with other particles[57].

Rheological and light scattering results by Hoffman[58,59]suggested that the shear thickening is due to shear induced order-disorder transition, associated with disruption of the layered structure at sufficiently high shear rates and thus destabilizing the flow. Repulsive interactions are

assumed to stabilize the layered structure. Hence, the onset of shear thickening is related to a critical shear rate above which the hydrodynamic lubrication forces exceed the electrostatic forces and particles deviate from the alignment, which results in enhanced interparticle interactions and thus higher viscosity[60]. However the order-disorder transition model has been disproved by rheo-optical and small angle neutron scattering (SANS) measurements of the shear thickened microstructure[61,62,6364]. Furthermore, Chow and Zukoski[65] investigated the shear thickening behavior of electrostatically stabilized particles in very thin rheometer gaps and found that the critical shear rate for shear thickening increases with increasing the gap size, indicating formation of gap-spanning clusters. These results suggested that the shear thickening is due to flow-induced formation of transient particle clusters, referred to as hydroclusters. The increase in viscosity is attributed to the anisotropic shape of the clusters and the enhanced effective particle volume fraction due to trapped solvent. The hydroclusters can collide with each other and thus "jam" the flow, leading to discontinuous shear thickening at a critical shear stress. If the particle volume fraction is not high enough, hydrocluster formation does not lead to jamming and the shear thickening effect is less pronounced. Formation of hydroclusters is controlled by the balance of hydrodynamic force needed to push particles together and the repulsive thermodynamic forces. This hydrocluster mechanism is in agreement with Stokesian dynamic simulations on hard-sphere dispersions, suggested by Bossis and Brady[66,67,68]. Based on this hydrodynamic model Bender and Wagner[63] suggested a scaling law for the onset of shear thickening and showed that it scales with shear stress, not shear rate. They expressed a dimensionless critical stress based on two-particle force balance between hydrodynamic lubrication force (with mean-field correction) and Brownian force. This scaling predicted that shear thickening sets in at a critical shear stress $\sigma_c \sim a^{-3}$, which is consistent with experimental data on hard sphere dispersions. On the other hand experimental results on repulsive Browninan particles revealed an a^{-2} dependence of the critical shear stress σ_c [57,69] (see Figure 1.25). This is explained with the strong repulsive forces, which act to resist the cluster formation. Indeed, considering the balance between hydrodynamic and electrostatic forces, as proposed by Boersma et al.[60], the particle size dependence of the dimensionless critical shear stress is reduced[69] but still fail to explain the experimental results.

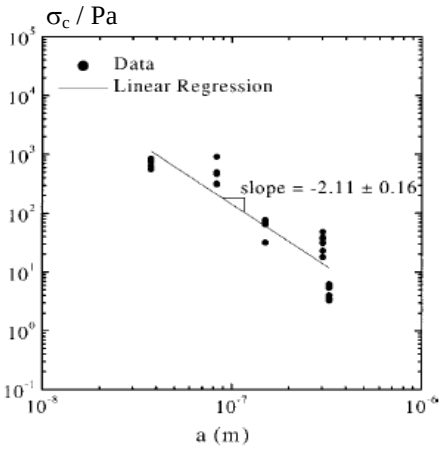

[Fig_025]

Figure 1.25 Critical shear stress σ_c versus particle radius a, for charge stabilized silica dispersions with various particle sizes and at different concentration ϕ=0.31 – 0.59. The line fits the power law dependence $\sigma_c \sim a^{-2}$. Adapted from Maranzano and Wagner[69]

Another approach to express the dynamics of hydrocluster formation is proposed by Melrose and Ball[70]. They related the critical shear rate to the characteristic relaxation time for two particles to "decouple" due to repulsive forces. Thereby a dimensionless critical shear rate has been expressed relating the convection time (inversely proportional to the shear rate) to the characteristic relaxation time. The results of this analysis are corrected, applying the mean field approximation proposed by Bender and Wagner[63] to account for the many-body hydrodynamic interactions, which tend to stabilize the hydrocluster structure[69]. In this manner a dimensionless critical stress σ_c^M for shear thickening has been derived:

[eq_047]

Equation 1.47

$$\sigma_c^M = \frac{3\pi\sigma_c a^2 / 2h_m}{2\pi\varepsilon_0\varepsilon_r\psi_s\kappa^2 a \dfrac{e^{-\kappa h_m}}{\left(1+e^{-\kappa h_m}\right)^2}}$$

Here ε_0 and ε_r are the permittivity in vacuum and the relative dielectric constant of the medium respectively, ψ_0 is the surface potential and κ is the reciprocal Debye length. The characteristic separation distance h_m indicates the particle separation distance at which the shear force balances the repulsive electrostatic force. It has been shown that the dimensionless critical shear stress

σ_c^M scales the experimental data for electrostatically[69] (see Figure 1.26) as well as sterically stabilized particles[71]. Note that the shear thickening sets in at a critical shear stress σ_c almost independent of particle volume fraction ϕ, while the corresponding critical shear rate $\dot{\gamma}_c = \sigma_c / \eta(\phi)$ decreases with increasing ϕ.

Shear thickening can be suppressed or shifted to higher critical stresses by broad particle size distribution[57]. It has been shown that for bimodal mixtures with size ratio $\chi \approx 3$ the critical shear stress σ_c increases with increasing volume fraction of small particles ξ_s [63,69].

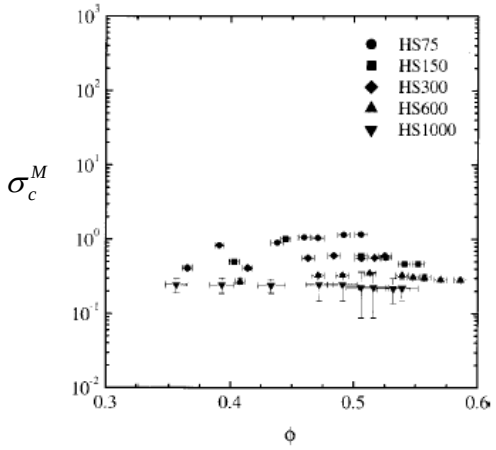

[Fig_026]

Figure 1.26 Dimensionless critical shear stress σ_c^M versus particle volume fraction ϕ for charge stabilized silica dispersions with various particle sizes: 75, 150, 300, 600, 1000 nm. Adapted from Maranzano and Wagner[69]

Particle shape can also influence the shear thickening behavior. Beazley[72] demonstrated that anisotropic clay suspensions exhibit shear thickening behavior at lower volume fractions and the effect increases with increasing the aspect ratio. Bergstrom[73] investigated aqueous suspensions of rod-shaped silicon carbide whiskers with aspect ratio $r_p \sim 10$ and reported shear thickening behavior at volume fraction as low as 17%. More recently, Egres and Wagner[74] investigated systematically the effect of particle anisotropy on the shear thickening using a poly(ethylene glycol) based suspensions of acicular precipitated calcium carbonate (PCC) particles with aspect ratio varying between 2 and 7. They found similar features of the rheological behavior of anisotropuc particles as for hard sphere dispersions. However two important results have been pointed out: the critical volume fraction for the onset of shear thickening decreases with increasing the aspect ratio but the critical shear stress σ_c is independent of the aspect ratio and

follows the scaling laws proposed for hard sphere dispersions with size corresponding to the minor axis dimension.

1.5 Rheology of Emulsions

The rheology of emulsions exhibits many qualitative analogues to the rheology of solid spherical particle dispersions. Differences arise from the deformability of liquid drops, which is especially relevant at high shear rates and volume fraction of the disperse phase. However, even at low shear rates the relative viscosity of emulsions differs from that of solid sphere dispersions. This is due to circulation of the flow inside the droplets which leads to deformation of the external streamlines around the fluid spheres such that the flow is less disturbed and viscous dissipation is lower[75]. The degree of streamline deformation depends on the viscosity ratio M:

[eq_048]

Equation 1.48

$$M = \frac{\eta_d}{\eta_s}$$

where η_d is the viscosity of the droplet liquid. For high droplet viscosity the viscosity ratio M approaches infinity and the distortion of the stream lines approaches that of rigid spheres. This effect is measurable even in very dilute emulsions and is captured by the Taylor equation[76]:

[eq_049]

Equation 1.49

$$\eta = \eta_s \left[1 + \left(\frac{1 + 2.5M}{1 + M} \right) \phi \right]$$

which reduces to the Einstein equation (Equation 1.28) for $M \to \infty$. Taylor's hydrodynamic theory assumes no deformation of droplets, which is satisfied at low enough shear rates. In typical oil-water emulsions the interfacial tension Γ is high enough to counteract the effect of hydrodynamic forces and leads to fast shape relaxation even at relative high shear rates. The droplet relaxation time τ_d is given by:

[eq_050]

Equation 1.50

$$\tau_d = \frac{a\eta_s}{\Gamma}$$

Mechanical deformation and rupturing of droplets occurs when the deformation time (inversely proportional to the shear rate) is exceeds the droplet relaxation time τ_d, which can be described by dimensionless Capillary number (see chapter 4 in volume 1 of "Product Design and Engineering"[20])

Experimental results on model emulsions of different viscosity ratios M, reported by Nawab and Mason[77] demonstrated an excellent agreement with Taylor's hydrodynamic theory (see Figure 1.26). Nawab and Mason pointed out that in some cases adsorbed surfactant layers can reduce the internal circulations and thereby cause an increase of intrinsic viscosity to the rigid sphere limit.

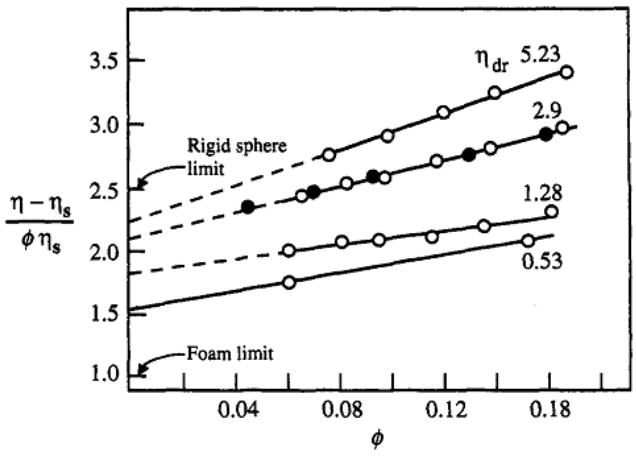

[eq_027]

Figure 1.27 Intrinsic viscosity versus droplet volume fraction for monodisperse emulsions of butyl benzoate oil droplets in different water solutions in order to vary the viscosity ratio M[77] (From Macosko, Rheology Principles, Measurements, and Applications, Copyright © 1994 John Wiley & Sons.)

With increasing concentration above the Einstein limit, hydrodynamic interaction become significant and Taylor's equation cannot describe the volume fraction – viscosity dependence. Pal [78] has proposed a new viscosity equation for concentrated emulsions that takes into account the effect of viscosity ratio M and reduces to the generalized Krieger-Dougherty equation (Equation 1.30)when $M \rightarrow \infty$:

[eq_051]

Equation 1.51

$$\eta_r \left[\frac{2\eta_r + 5M}{2 + 5M} \right]^{3/2} = \left[1 - \frac{\phi}{\phi_{\max}} \right]^{-2.5\phi_{\max}}$$

Pal[78] also showed that Equation 1.51 is in a good agreement with the experimental data for various of emulsions over a broad range of droplet volume fraction ϕ and viscosity ratios M.

The effect of dispersed phase volume fraction on rheology of emulsions is less severe in comparison to dispersions of solid particles. Emulsions behave as Newtonian fluids up to volume fraction of closest packing of nondeforamble hard spheres $\phi \approx 0.6$. At higher concentrations emulsions show a strong shear thinning behavior and the effect increases with droplet volume fraction[79]. Furthermore, in the high concentration limit ($\phi > 0.6$) the effect of droplet size becomes significant. Reducing the droplet size viscosity of concentrated emulsions considerably increase and the shear thinning effect get stronger[79]. It should be mentioned that increasing the volume fraction of the dispersed phase not necessarily results in a monotonic increase in viscosity. At critical droplet volume fraction phase inversion may occur which is accompanied by a drastic drop in viscosity. However emulsions are usually stabilized by surfactants adsorbed onto droplet surface that prevent the coalescence of droplets at contact.

Repulsive and attractive colloidal interactions as well as droplet deformation and rupture during flow can cause a deviation from the hard sphere behavior of emulsions. The effect of repulsive droplet interactions due to surface charge or adsorbed polymer can be captured by hard sphere mapping ($\phi = \phi_{eff}$) similar as for repulsive solid particles. Attractive droplet interactions lead to flocculation and gelation analogous to attractive particle suspensions. Emulsion rheology can be tuned in a wide range by adding polymer thickeners or by excess surfactant providing gel-like structure to the continuous phase, which is particularly relevant for stabilization against creaming.

Emulsions can exhibit distinct viscoelastic properties even if both constituents are Newtonian fluids due to the contribution of the interfacial tension which oppose droplets deformation. This is particularly important for polymer blends, where viscosity of both components is high and deformed interfaces relax slowly. Various models have been established to describe the liner viscoelastic complex shear modulus G* of emulsions. When both phases are Newtonian the Oldroyd model[80],[81] suits:

[eq_052]

Equation 1.52

$$G^* = i\omega\eta_s\left(\frac{1+\frac{3}{2}\phi\frac{E}{D}}{1-\phi\frac{E}{D}}\right)$$

with

[eq_053]

Equation 1.53

$$E = 2i\omega(\eta_d - \eta_s)\,(19\eta_d + 16\eta_s) + \frac{8\Gamma}{a}(5\eta_d + 2\eta_s)$$

$$D = i\omega(2\eta_d + 3\eta_s)(19\eta_d + 16\eta_s) + \frac{40\Gamma}{a}(\eta_d + \eta_s)$$

For emulsions with viscosity ratio M $\rightarrow \infty$ droplets behave as solid-like particles and the droplet relaxation time is so short that ratio E/D reduces to:

[eq_054]

Equation 1.54

$$\frac{E}{D} = \frac{0.4 + M}{1 + M}$$

In the dilute limit with $\phi \rightarrow 0$, Equation 1.52 simplifies to:

[eq_055]

Equation 1.55

$$G^* = i\omega\eta_s\left(1+\frac{5}{2}\phi\frac{E}{D}\right)$$

For emulsions where both continuous and dispersed phase are viscoelastic with frequency dependent complex moduli G_s^* and G_d^* respectively, the Palierne[82] model gives the following comlex modulus G* of the emulsions:

[eq_056]

Equation 1.56

$$G^* = G_s^* \left(\frac{1 + \frac{3}{2}\phi \frac{E}{D}}{1 - \phi \frac{E}{D}} \right)$$

with

[eq_057]

Equation 1.57

$$E = 2\left(G_d^* - G_s^*\right)\left(19G_d^* + 16G_s^*\right) + \frac{8\Gamma}{a}\left(5G_d^* + 2G_s^*\right)$$

$$D = \left(2G_d^* + 3G_s^*\right)\left(19G_d^* + 16G_s^*\right) + \frac{40\Gamma}{a}\left(G_d^* + G_s^*\right)$$

Kitade et al[83] investigated the viscoelastic properties of polymer blends consisting of polydimethylsiloxane (PDMS) and polyisoprene and demonstrated that the experimentally determined frequency dependence of G′ is in agreement with the Palierne model (see Figure 1.28). The contribution of the interfacial term results in a pronounced shoulder in the G′ (ω) curve in the low frequency range. Figure 1.28 shows that with increasing the pre-shear rate, which corresponds to a decrease of the average droplet size[83], the “shoulder” in the G′ (ω) dependence shifts to higher frequencies. This is due to increased interfacial area and hence more pronounced interfacial contribution for smaller droplets. In the high frequency limit the interfacial terms can be ignored and G′ is determined only by the viscoelasticity of the dispersion medium. Hence, the Palierne emulsion model simplifies to:

[eq_058]

Equation 1.58

$$G^* \approx (1 - \phi)G_s^* + \phi G_d^*$$

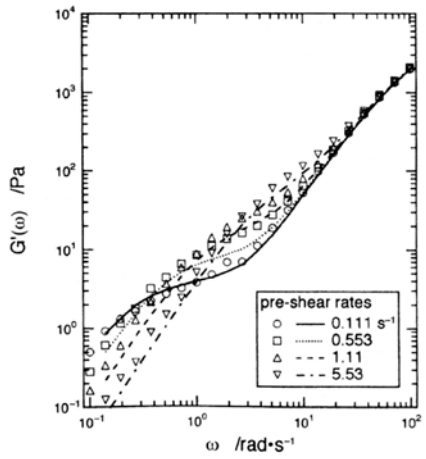

[Fig_028]

Figure 1.28 Comparison of the Palierne model (lines) with measured G′ (ω) dependence for a blend of 11% polyisoprene (η_0 = 60.9 Pas) in PDMS (η_0 = 73.7 Pas) with Γ=3.2 mN/m, pre-sheared at four different shear rates[83]

Below a critical volume fraction ϕ_c, which can be associated with the colloidal glass transition or random close packing, rheology of emulsions is dominated by Brownian motion, hydrodynamic and colloidal interactions. Above ϕ_c droplets begin to deform and take a polyhedral form via compression. The so formed foam-like structure behave predominantly elastic. A thermodynamic model developed by Princen[84] related the droplet compression to the osmotic pressure in the system which increases with increasing droplet volume fraction ϕ. When the osmotic pressure exceeds the Laplace pressure, Γ/a, droplets start to deform and pack more tightly with increasing ϕ. Elasticity of the system then arises from the surface tension acting to resist the compression (osmotic pressure). Such a highly concentrated emulsion behave as a linearly elastic solid with G′>G″, independent of frequency. The plateau modulus G_0 of densely packed emulsions strongly increases with droplet volume fraction and can be expressed as follows[85]:

[eq_059]

Equation 1.59

$$G_0 = \frac{3\Gamma}{2a}\left(\phi_{eff} - \phi_c\right)$$

where ϕ_{eff} accounts for the excluded volume due to repulsive forces. When ϕ_{eff} approaches unity the G_0 becomes constant determined by $\Gamma/2a$.

Densely packed emulsions with $\phi > \phi_c$ are characterised by an apparent yield stress σ_y at which the structure ruptures. Oscillatory measurements revealed that yielding occurs at a critical deformation amplitude, called yield strain $\gamma_y = \sigma_y / G_0$, that increases linearly with increasing droplet volume fraction above ϕ_c[86]:

[eq_060]

Equation 1.60

$$\gamma_y \sim \left(\phi_{eff} - \phi_c\right)$$

Figure 1.29a demonstrates this linear dependence for monodispersed emulsions having different droplet size. It can be seen that the volume fraction dependence of γ_y is independent of droplet size and γ_y reaches its minimum at ϕ_c. In contrast to the yield strain γ_y, the yield stress σ_y increases more severely (see Figure 1.29b). The yield stress σ_y scales with the Laplace pressure of the droplets and can be empirically fit by:

[eq_061]

Equation 1.61

$$\sigma_y \sim \left(\phi_{eff} - \phi_c\right)^2$$

This quadratic dependence of σ_y on ϕ_{eff} is consistent with the definition $\sigma_y = \gamma_y G_0$. and for $\phi_{eff} \approx 1$ a crude estimate holds:

[eq_062]

Equation 1.62

$$\sigma_y\left(\phi_{eff} = 1\right) \approx 0.1\frac{\Gamma}{a}$$

These experimental findings are captured by the Princes-Kiss model[87]:

[eq_063]

Equation 1.63

$$\sigma_y = \frac{\Gamma}{a}\phi^{1/3}Y(\phi)$$

where Y(ϕ) can be expressed in analytical form for two-dimensional systems, however for real three-dimensional emulsions is Y(ϕ) an empirical function.

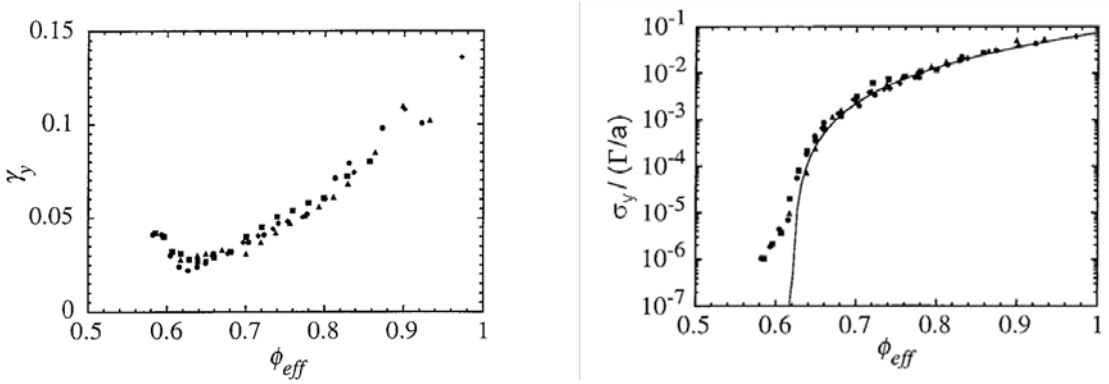

[Fig_029]

Figure 1.29a–b a Yield strain γ_y versus effective volume fraction ϕ_{eff} **b** yield stress σ_y scaled by the Laplace pressure (Γ/a) versus ϕ_{eff} for monodispersid emulsions with droplet size: a = 250 nm (circles), 370 nm (triangles), 530 nm (squares) and 740 nm (diamonds)[86]

Highly concentrated emulsions often do not exhibit uniform deformation even in simple shear flow, instead they show shear banding which can be very irregular in sense that the plane of deformation changes its position or that the width of the deformed region changes with time.

References

[1] Geisekus H. and Langer G., "Die Bestimmung der wahren Fliesskurven nicht-newtonscher Flüssigkeiten und plastischer Stoffe mit der Methode der repräsentativen Viskosität", Rheol. Acta, 16 (1997) 1

[2] Macosko C. W., "Rheology Principles, Measurements, and Applications", Wiley - VCH Publishers, New York, 1994

[3] Schümmer P, Worthoff R. H: "An Elementary Method for the Evaluation of the Flow Curve", Chem. Eng. Sci. 33 (1978) 759

[4] Bagley E. B "End Corrections in the Capillary Flow of Polyethylene", J. Appl. Phys., 28 (1957) 624

[5] Mooney ., "Explicit formulas for slip and fluidity", J. Rheol., 2 (1931) 210

[6] Laun, H. M., "Rheological properties of aqueous polymer dispersions", Angew. Makromol. Chem. 123/124 (1984) 335

[7] Einstein A., "Eine neue Bestimmung der Moleküldimensionen", Ann. Phys 19 (1906) 289

[8] Einstein A. "Berichtigung zu meiner Arbeit: Eine neue Bestimmung der Moleküldimensionen"Ann. Phys 34 (1911) 591.

[9] Batchelor, G. K., "The effect of Brownian motion on the bulk stress in a suspension of spherical particles", J. Fluid Mech.,83 (1977) 97.

[10] Krieger I. M., Dougherty T. J., "A mechanism for non-Newtonian flow in suspensions of rigid spheres", Trans. Soc. Rheol., 3 (1959) 137

[11] Quemada D., "Rheology of concentrated disperse systems and minimum energy dissipation principle I. Viscosity-concentration relationship", Rheol. Acta., 16 (1977) 82

[12] Buscall R., D'Haene P., Mewis J., "Maximum density for flow of dispersions of near monodisperse spherical-particles" Langnuir, 10 (1994) 1439

[13] Pusey P. N., van Megen W., "Phase behavior of concentrated suspensions of nearly hard colloidal spheres", 320 (1986) 340

[14] van Megen W., Underwood S. M., "Glass transition in colloidal hard spheres: Measurement and mode-coupling-theory analysis of the coherent intermediate scattering function", Phys. Rev. E, 49 (1994) 4206

[15] Meeker S. P., Poon W. C. K., Pusey P. N., "Concentration dependence of the low-shear viscosity of suspensions of hard-sphere colloids" Phys. Rev. E, 55 (1997) 5718

[16] Phan S.-E., Russel W. B., Cheng Z., Zhu J., "Phase transition, equation of state, and limiting shear viscosities of hard sphere dispersions" Phys. Rev. E 54 (1996) 6633

[17] Larson R. G. “The structure and rheology of complex fluids”, Oxford University Press, New York 1999

[18] Choi G. N., Krieger I. M., „Rheological studies on sterically stabilized model dispersions of uniform colloidal colloidal spheres 2. Steady-shear viscosity” 113 (1986) 101

[19] Brenner H., „Rheology of a dilute suspension of axisymmetric brownian particles“, Int. J. Multiphase Flow, 1 (1974) 195

[20] Bröckel U., Meier W., Wagner G., „Product design and engineering, Volume 1: Basics and Thechnologies”, Wiley - VCH Publishers, Weinheim, 2007

[21] Horn F.M., Richtering W., Bergenholtz J., Willenbacher N., Wagner N. J., „Hydrodynamic and colloidal interactions in concentrated charge-stabilized polymer dispersions, J. Colloid Interface Sci. 225 (2000) 166

[22] Fritz G., Schädler V., Willenbacher N., Wagner N. J., „Electrosteric stabilization of colloidal dispersions“, Langmuir 18 (2002) 6381

[23] Wetz D.A, Oliveria M., „Fractal structures formed by kinetic aggregation of aqueous gold colloids“, Phys. Rev. Lett., 52 (1984) 1433

[24] Weitz D.A., Huang J. S., Lin M.Y., Sung J., „Limits of the fractal dimensions for irreversible kinetic aggregation of gold colloids”, Phys. Rev. Lett.,54 (1985) 1416

[25] Sonntag R.C., Russel W.B., „Structure and breakup of flocs subjected to fluid stresses: I. Shear experiments”, J. Colloid Interface Sci. 113 (1986) 399

[26] Woutersen A.T.J.M. , de Kruif C.G. “The rheology of adhesive hard-sphere dispersions”, J. Chem. Phys. 94 (1991) 5739

[27] Buscall, R., McGowan J. I., Morton-Jones A. J., ‘‘The rheology of concentrated dispersions of weakly-attracting colloidal particles with and without wall slip’’, J. Rheol., 37 (1993) 621

[28] Tadros T. F., “Rheology of dispersions – Principles and application”, Wiley-VCH, Weinheim Publishers, 2010

[29] Buscall R., Mills P.D.A, Yates G.E., “Viscoelastic properties of strongly flocculated polystyrene latex dispersions”, Colloids and Surfaces, 18 (1986) 341

[30] Buscall R., McGowan I.J., Mills P.D.A., Stewart R.F., Sutton D., White L.R., Yates G.E.,“The rheology of strongly flocculated suspensions”, J. Non-Newtonian Fluid Mech., 24 (1987) 183

[31] Buscall R., Mills P.D.A., Goodwin J.W., Lawson D.W., ‘‘Scaling behavior of the rheology of aggregate networks formed from colloidal particles’’, J. Chem. Soc. Faraday Trans. 84 (1988) 4249

[32] Tadros T.F., “Correlation of viscoelastic properties of stable and flocculated suspensions with their interparticle interactions”, Adv. Colloid Interface Sci., 68 (1996) 97

[33] Koos E., Willenbacher N., „Capillary forces in suspension rheology” Science, 331 (2011) 897

[34] Fabbian L., Gotze W., Sciortino F. Tartaglia P., Thiery F., “Ideal glass-glass transitions and logarithmic decay of correlations in a simple system”, Phys. Rev. E, 59 (1999) R1347

[35] Fabbian L., Gotze W., Sciortino F. Tartaglia P., Thiery F., “Erratum: Ideal glass-glass transitions and logarithmic decay of correlations in a simple system [Phys. Rev. E 59, R1347 (1999)], Phys. Rev. E, 60 (1999) 2430

[36] Dawson K., Foffi G., Fuchs M., Götze W, Sciortino F., Sperl M., Tartaglia P., Voigtmann Th., Zaccarelli E., Higher-order glass-transition singularities in colloidal systems with attractive interactions”, Phys. Rev. E, 63 (2000) 011401

[37] Pham K.N. Puertas A.N., Bergenholtz J., Egelhaaf S.U., Moussaidl A., Pusey P.N., Schofield A.B., Cates M.E., Fuchs M., Poon W.C.K., “Multiple glassy state in a simple model system”, Science, 296 (2002) 104

[38] Pham K. N., Egelhaaf S. U., Pusey P. N., Poon W. C. K., “Glasses in hard spheres with short-range attraction”, Phys. Rev. E, 69 (2004) 011503

[39] Eckert T., Bartsch E. “Re-entrant glass transition in a colloid-polymer mixture with depletion attractions” Phys. Rev. Lett.,89 (2002) 125701

[40] Eckert T., Bartsch E., “Glass transition dynamics of hard sphere like microgels colloids with short-ranged attractions”, J. Phys. Condens. Matter, 16 (2004) S4937

[41] Eckert T., Bartsch E., “Glass transition dynamics of hard sphere like microgel colloids with short-ranged attractions”, J. Phys. Condens. Matter, 16 (2004) S4937

[42] Gopalakrishnan V., Zukoski C.F., “Effect of attractions on shear thickening in dense suspensions”, J. Rheol, 48 (2004) 1321

[43] Krishnamurthy L.N., Wagner N. J., “The influence of weak attractive forces on the microstructure and rheology of colloidal dispersions”, J. Rheol, 49 (2005) 457

[44] Dawson K.A.,“The glass paradigm for colloidal glasses, gels, and other arrested states driven by attractive interactions”, Curr. Opin. Colloid Interface Sci., 7 (2002) 218

[45] Eckert T., Bartsch E., “Re-entrant glass transition in a colloid-polymer mixture with depletion attractions”, Phys. Rev. Lett. 89 (2002) 125701

[46] Willenbacher N., Vesaratchanon J. S., Thorwarth O., Bartsch E., “An alternative route to highly concentrated, freely flowing colloidal dispersions”, Soft Matter, 7 (2011) 5777

[47] Farris R.J., “Prediction of the viscosity of multimodal suspensions from unimodal viscosity data”, Trans. Soc. Rheol., 12 (1968) 281

[48] Chong J.S., Christiansen E.B., Baer A.D., “Rheology of concentrated suspensions”, J. Appl. Polym. Sci., 15 (1971) 2007

[49] Rodriguez B.E., Kaler E.W., Wolfe M.S., “Binary mixtures of monodisperse latex dispersions 2. Viscosity”, Langmuir 8 (1992) 2382

[50] McGeary R.K., “Mechanical packing of spherical particles“, J. American Ceramic Soc. 44 (1961) 513

[51] Dames B., Morrison B.R:, Willenbacher N., “An empirical model predicting the viscosity of highly concentrated, bimodal dispersions with colloidal interactions“, Rheol. Acta, 40 (2001) 434

[52] Bartlett P., Pusey P.N., “Freezing of binary mixtures of hard-sphere colloids”, Physica A, 194 (1993) 415

[53] van Duijneveldt J.S., Heinen A.W., Lekkerkerker H.N.W., 2Phase separation in bimodal dispersions of stercally stabilized silica particles” Europhys. Lett. 21 (1993) 369

[54] Hunt W.J., Zukoski C.F., The equilibrium properties and microstructure of mixtures of colloidal particles with long-range, soft repulsions”, J. Colloid Interface Sci., 210 (1999) 332

[55] Gondret P., Petit L., “Viscosity of bimodal suspensions”, J. Rheol., 41 (1997) 1261

[56] Sudduth, R.D.,“A generalized model to predict the viscosity of solutions with suspended particles I“, J. Appl. Polym. Sci., 48 (1993) 25

[57] Barnes H.A., “Shear-thickening (“Dilatancy“) in suspensions of nonagregating solid particles dispersed in newtonian liquids”, J. Rheol. ,33 (1989) 329

[58] Hoffman R.L., “Discontinuous and dilatant viscosity behavior in concentrated suspensions I. Observation of a flow instability”, Trans. Soc. Rheol., 16 (1972) 155

[59] Hoffman R.L., “Discontinuous and dilatant viscosity behavior in concentrated suspensions II. Theory and experimental tests”, J. Chem. Phys., 46 (1974) 491

[60] Boersma W.H., Laven J., Stein H.N., “Shear thickening (dilatancy) in concentrated suspensions”, AIChE J., 36 (1990) 321

[61] Laun H.M., Bung R., Schmidt F., “Rheology of extremely shear thickening polymer dispersions (passively viscosity switching fluids)”, J. Rheol., 35 (1991) 999

[62] Laun H.M., Bung R., Hess S., Loose W., Hahn K., Hadicke E., Hingmann R.,Schmidt F., Lindner P., “Rheological and small angle neutron scattering investigation of shear-induced particle structures of concentrated polymer dispersions”, J. Rheol., 36 (1992) 743

[63] Bender J., Wagner N.J., “Reversible shear thickening in monodisperse and bidisperse colloidal dispersions“, J. Rheo, 40 (1996) 899

[64] Bender J.W., Wagner N.J. “Optical measurement of the contributions of colloidal forces to the rheology of concentrated suspension”, J. Colloid Interface Sci. 172 (1995) 171

[65] Chow M.K., Zukuski C.F., “Gap size and shear history dependencies in shear thickening of a suspension ordered at rest”, J. Rheo., 39 (1995) 15

[66] Brady J.F., Bossis G., “Stokesian dynamics”, Ann Rev Fluid Mech., 20 (1988) 111

[67] Brady J.F., Bossis G., “The rheology of Brownian suspensions”, J. Chem. Phys., 91 (1989) 1866

[68] Phung T.N., Brady J.F., Bossis G., “Stokesian Dynamics simulation of Brownian suspensions”, 313 (1996) 181

[69] Maranzano B.J., Wagner N.J., “The effect of particle size on reversible shear thickening of concentrated colloidal dispersions”, J. Chem. Phys., 114 (2001) 10514

[70] Melrose J.R., Catherall A.A., Ball R.C., “Shear thickening and order-disorder effects in concentrated colloids at high shear rates”, J. Rheol., 44 (2000) 1

[71] Krishnamurthy L.N., Wagner N. J., “Shear thickening in polymer stabilized colloidal dispersions”,J. Rheol., 49 (2005) 1347

[72] Beazley K.M., “Industrial aqueous suspensions“ in “Rheometry: industrial applications” edited by K. Walters, Research Studies Press, Chichester ,1980

[73] Bergstrom L., “Shear thinning and shear thickening of concentrated ceramic suspensions“, Colloids Surf., A, 133 (1998) 151

[74] Egres R.G., Wagner N.J., “The rheology and microstructure of acicular precipitated calcium carbonate colloidal suspensions through the shear thickening transition”, J. Rheol, 49 (2005) 719

[75] Bartok W., Mason S.G., “Particle motions in sheared suspensions: VII. Internal circulation in fluid droplets (theoretical)”, J. Colloid Interface Sci., 13 (1958) 293.

[76] Taylor G.I., „The viscosity of a fluid containing small drops of another fluid”, Proc. R. Soc., A, 138 (1932) 41

[77] Nawab, M.A., Mason S.G., “The viscosity of diluted emulsions”, Trans. Faraday Soc., 54 (1985) 1712

[78] Pal R., “Novel viscosity equations for emulsions oft wo immiscible liquids“, J. Reol., 45 (2001) 509

[79] Pal R., “Shear viscosity behavior of emulsions of two immiscible liquids”, J. Colloid Interface Sci., 225 (2000) 359

[80] Oldroyd J.G., “The elastic and viscous properties of emulsions and suspensions”, Proc. R. Soc. A, 218 (1953) 122

[81] Oldroyd J.G., ”The effect of interfacial stabilizing films on the elastic and viscous properties of emulsions”, Proc. R. Soc. A, 232 (1955) 567

[82] Palierne J.F., “Linear rheology of viscoelastic emulsions with interfacial tension”, Rheol. Acta, 29 (1990) 204

[83] Kitade S., Ichikawa A., Imura M., Takahashi Y., Noda I., “Rheological properties and domain structures of immiscible polymer blends under steady and oscillatory shear flows”, J. Rheo. 41 (1997) 1039

[84] Princen H.M., “Osmotic pressure of foams and highly concentrated emulsions. 1. Theoretical considerations”, Langmuir, 2 (1986) 519

[85] Mason T.G., Lacasse M-D., Grest S.G., Levine D., Bibette J., Weitz D.A., “Osmotic pressure and viscoelastic shear moduli of concentrated emulsions”, Phys. Rev. E, 56 (1997) 3150

[86] Mason T.G., Bibette J., Weitz D.A., “Yielding and flow of monodisperse emulsion“,J. Colloid Interface Sci., 179 (1996) 439

[87] Princen H.M., Kiss A.D., “Rheology of foams and highly concentrated emulsions: 3. Static shear modulus”, J Colloid Interface Sci, 112 (1986) 427